Pergamon

*Int. J. Multiphase Flow* Vol. 20, No. 1, pp. 185–210, 1994

0301-9322/94 $6.00 + 0.00

# SLOW MOTION OF AN ARBITRARY AXISYMMETRIC BODY ALONG ITS AXIS OF REVOLUTION AND NORMAL TO A PLANE SURFACE

H. J. KEH and C. H. TSENG
Department of Chemical Engineering, National Taiwan University, Taipei 106-17, Taiwan, R.O.C.

*(Received 18 November 1992; in revised form 12 August 1993)*

**Abstract**—This paper presents a combined analytical-numerical study for the Stokes flow caused by an arbitrary body of revolution translating axisymmetrically in viscous fluid toward an infinite plane, which can be either a solid wall or a free surface. A singularity method based on the principle of distribution of a set of Sampson spherical singularities along the axis of revolution within a prolate body or on the fundamental plane within an oblate body is used to find the general solution for the fluid velocity field which satisfies the boundary condition at the infinite plane. The no-slip condition on the surface of the translating body is then satisfied by applying a boundary collocation technique to this general solution to determine the unknown coefficients. The hydrodynamic drag exerted on the body is evaluated with good convergence behavior for various cases of the body shape and the separation between the plane and the body. For the motion of a sphere normal to a solid plane or a planar free surface, our drag results agree very well with the exact solutions obtained by utilizing spherical bipolar coordinates. For the translation of a spheroid, prolate or oblate, along its axis of symmetry and perpendicular to a plane wall, the agreement between our results and the numerical solutions obtained using the boundary integral method is also quite good. In addition to the solutions for a spheroidal body, the drag results for the axially symmetric motions of a Cassini oval towards a solid plane and a planar free surface are also presented.

*Key Words:* axisymmetric creeping flow, body of revolution, boundary effect, spheroid, Cassini oval

## 1. INTRODUCTION

The application of hydrodynamic theory to the behavior of particles moving in a viscous fluid at low Reynolds numbers has continued to receive much attention from investigators in the fields of chemical and biomedical engineering and science. The majority of these particle phenomena are fundamental in nature, but permit one to develop rational understanding of many practical systems and industrial processes such as sedimentation, flotation, spray drying and the motion of red blood cells in an artery or vein. A summary for the current state of knowledge in this area is given in Kim & Karrila (1991).

The theoretical treatment of this subject has grown out of the work of Stokes (1851) for a translating sphere. Oberbeck (1876) extended this result to the translation of an ellipsoid. More recently, solutions of the creep-flow problem have been derived for bodies which correspond to a coordinate surface of one of the special orthogonal coordinate systems in which the Stokes equations are simply separable (Payne & Pell 1960; Goren & O'Neill 1980) and for long slender bodies (Batchelor 1970; Cox 1970). Additionally, the low-Reynolds-number flow caused by the motion of a particle of more general shape in an unbounded fluid has also been treated in the literature by the truncated-series boundary-collocation method (Gluckman *et al.* 1972), the singularity method (Chwang & Wu 1975) and the boundary integral method (Youngren & Acrivos 1975; Weinbaum *et al.* 1990; Pozrikidis 1992).

In most technical applications, particles are not isolated and the surrounding fluid is externally bounded by solid or fluid surfaces. Thus, it is important to determine if the presence of neighboring boundaries significantly affects the movement of particles. Through an exact representation in spherical bipolar coordinates, the motion of a spherical particle normal to an infinite planar surface was independently analyzed by Maude (1961) and Brenner (1961). The translation and rotation of a sphere on which a constant force and/or torque is applied parallel to a plane wall was investigated by O'Neill (1964) using bipolar coordinates. The boundary effects on the motion of

a sphere were also examined for many other geometries such as in a long circular tube (Haberman & Sayre 1958), between two parallel plates (Ganatos *et al.* 1980), along the axis of a finite disk (Dagan *et al.* 1982) and near a circular orifice (Yan *et al.* 1987).

On the other hand, the slow motion of a nonspherical particle next to a plane wall has been studied for several cases. Using cylindrical bipolar coordinates, the two-dimensional creeping motion of a circular cylinder near a plane wall was analyzed by Jeffrey & Onishi (1981) and Keh *et al.* (1991). Dabros (1985) applied a technique of internal distribution of Stokeslets and potential sources to calculate the angular velocity of a prolate spheroid adjacent to a rigid plane wall. The axisymmetric flow induced by the motion of an arbitrary prolate body of revolution normal to a rigid plane wall was treated by Yuan & Wu (1987) using a method of internal distribution of spherical singularities combined with the boundary-collocation technique. Recently, Hsu & Ganatos (1989) solved for the motion of an arbitrarily-shaped rigid body in Stokes flow adjacent to a rigid plane wall using the boundary integral equation method.

In this paper we use the method of distributed internal singularities incorporated with the bounded-flow collocation technique developed by Yuan & Wu (1987) to analyze the axisymmetric creeping flow generated by an arbitrary body of revolution translating along its axis of symmetry and prependicular to a plane surface. Differing from their work, the translating body can be either prolate or oblate and the plane surface can be either a solid wall or a free surface here. The drag force exerted on the body by the fluid as a function of the relative separation between the body and the plane is calculated for various body shapes: a sphere; a spheroid; and a Cassini oval. For the cases of a sphere and a spheroid, our drag reuslts show excellent agreement with the exact solutions derived by Maude (1961) and Brenner (1961) and with the numerical calculations obtained by Hsu & Ganatos (1989), respectively.

## 2. MATHEMATICAL DESCRIPTION OF THE PROBLEM

We consider the creeping motion caused by an arbitrary axisymmetric body translating with a constant velocity in an incompressible, Newtonian fluid along its axis of revolution and perpendicular to an infinite plane located at a distance $d$ from the center of the body. The fluid is at rest at infinity. The body is rigid and the planar boundary can be either a solid wall or a free surface. The circular cylindrical coordinates $(\rho, \phi, z)$ and the spherical coordinates $(r, \theta, \phi)$ are utilized and the body center is chosen to be the origin of the coordinates instantaneously, as shown in figure 1. The governing equations for the fluid motion are

$$\eta \nabla^2 \mathbf{v} - \nabla p = \mathbf{0} \qquad [1a]$$

and

$$\nabla \cdot \mathbf{v} = 0, \qquad [1b]$$

where $\eta$ is the fluid viscosity, $\mathbf{v}(\mathbf{x})$ is the fluid velocity and $p(\mathbf{x})$ is the dynamic pressure.

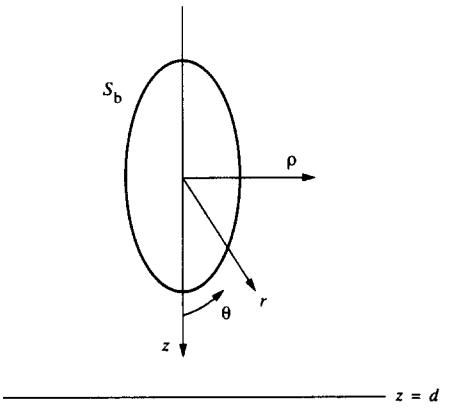


Figure 1. Motion of an arbitrary axisymmetric body along its axis of revolution and normal to an infinite planar boundary.

Owing to the axisymmetric nature of the flow, it is convenient to introduce the Stokes stream function $\Psi$ which satisfies [1b] and is given in cylindrical coordinates by

$$v_\rho = \frac{1}{\rho}\frac{\partial \Psi}{\partial z} \qquad [2a]$$

and

$$v_z = -\frac{1}{\rho}\frac{\partial \Psi}{\partial \rho}. \qquad [2b]$$

Here, $v_\rho$ and $v_z$ are the radial and axial components of the fluid velocity, respectively. Taking the curl of [1a] and applying [1b], as well as the definition of the stream function, give a fourth-order linear partial differential equation for $\Psi$:

$$E^4\Psi = E^2(E^2\Psi) = 0. \qquad [3]$$

In cylindrical coordinates, the axisymmetric Stokesian operator $E^2$ is given by

$$E^2 = \rho\frac{\partial}{\partial \rho}\left(\frac{1}{\rho}\frac{\partial}{\partial \rho}\right) + \frac{\partial^2}{\partial z^2}. \qquad [4]$$

Because the fluid velocity satisfies the no-slip requirement at the fluid/solid interfaces of the body and the wall and the fluid is motionless far away from the body, the boundary conditions for the case of the translation of a body toward a solid plane are:

$$\mathbf{v} = U\mathbf{e}_z \quad \text{on } S_b; \qquad [5a]$$

$$\mathbf{v} = \mathbf{0} \quad \text{at } z = d; \qquad [5b]$$

and

$$\mathbf{v} \to \mathbf{0} \quad \text{as } (\rho^2 + z^2)^{1/2} \to \infty \text{ and } z \leqslant d. \qquad [5c]$$

Here, $U$ is the velocity of the body, $\mathbf{e}_z$ is the unit vector in the axial direction and $S_b$ denotes the surface of the body. For the case that the body is moving toward a planar free surface, [5b] is replaced by

$$v_z = 0 \quad \text{and} \quad \frac{\partial v_\rho}{\partial z} = 0 \quad \text{at } z = d. \qquad [6a, b]$$

The deformation of the free surface produced by the approaching body will not be considered here, although it may not be neglected in some real situations involving heavy viscous liquids, especially for very close approach of the body to the free surface (Lee & Leal 1982).

The drag force $\mathbf{F}$ $(=F\mathbf{e}_z)$ exerted by the fluid on the surface of the axisymmetric body can be determined from (Happel & Brenner 1983)

$$F = \frac{\eta}{2}\int\int_{S_b} \rho^2 \mathbf{n}\cdot\nabla\left(\frac{1}{\rho^2}E^2\Psi\right) \mathrm{d}S, \qquad [7]$$

where $\mathbf{n}$ is a unit vector normal to the body surface $S_b$, pointing into the fluid.

To solve [3]–[6a, b], a set of Sampson spherical singularities (also called Sampsonlets) is chosen and distributed along the axis of revolution within a prolate body (Wu 1984; Yuan & Wu 1987) or on the fundamental plane within an oblate body (Zhu & Wu 1985). At first, the reflection of each Sampsonlet with respect to the planar boundary is ascertained by satisfying the boundary conditions [5c] and [5b] (for a solid plane) or [6a, b] (for a free surface). Then, the disturbance of the flow field generated by the body and the planar boundary is approximated by the superposition of the set of the planar reflection of the spherical singularities. Finally, boundary condition [5a] on the surface of the body can be satisfied by making use of the multipole collocation method. For the special case of a spherical body, only a single Sampsonlet which is placed at the body center is needed.

In the following section we shall derive the reflections of an arbitrarily-located Sampsonlet with respect to a solid plane and a planar free surface.

## 3. THE IMAGE OF A SAMPSONLET WITH RESPECT TO AN INFINITE PLANE

The stream function for the fluid motion caused by a Sampson spherical singularity at the point $\rho = 0$ and $z = h$ is (Sampson 1891)

$$\Psi_s = \sum_{n=2}^{\infty} [B_n B_n'''(\rho, z-h) + D_n D_n'''(\rho, z-h)], \quad [8]$$

where $B_n$ and $D_n$ are unknown constant coefficients,

$$B_n'''(\rho, z) = \frac{1}{(\rho^2+z^2)^{(n-1)/2}} G_n^{-1/2}\left[\frac{z}{(\rho^2+z^2)^{1/2}}\right] \quad [9a]$$

and

$$D_n'''(\rho, z) = \frac{1}{(\rho^2+z^2)^{(n-3)/2}} G_n^{-1/2}\left[\frac{z}{(\rho^2+z^2)^{1/2}}\right], \quad [9b]$$

and $G_n^{-1/2}$ is the Gegenbauer polynomial of the first kind of order $n$ and degree $-1/2$. When infinite plane is at $z = d$ ($d > 0$, $d > h$), the stream function for the region $z \leqslant d$ (containing the Sampsonlet at $\rho = 0$ and $z = h$) can be linearly decomposed into two parts:

$$\Psi = \Psi_w + \Psi_s. \quad [10]$$

Here $\Psi_w$ is a solution of [3] that represents the disturbance produced by the infinite plane and is given by a Fourier–Bessel integral,

$$\Psi_w = \int_0^{\infty} \rho J_1(\omega\rho)[X(\omega) + zY(\omega)]\, e^{\omega z}\, d\omega, \quad [11]$$

where $J_n$ is the Bessel function of the first kind of order $n$ and $X(\omega)$ and $Y(\omega)$ are unknown functions of $\omega$. $\Psi_s$, which is also a solution of [3], is given by [8]. Note that the boundary condition [5c] is immediately satisfied by a solution of the forms [8] and [11].

Substituting [8] and [11] into [10], one can apply relations [2a, b] to yield

$$v_\rho = \sum_{n=2}^{\infty} [B_n B_n'(\rho, z-h) + D_n D_n'(\rho, z-h)] - \int_0^{\infty} \omega J_1(\omega\rho) G^*(\omega, z)\, d\omega \quad [12a]$$

and

$$v_z = \sum_{n=2}^{\infty} [B_n B_n''(\rho, z-h) + D_n D_n''(\rho, z-h)] - \int_0^{\infty} \omega J_0(\omega\rho) F^*(\omega, z)\, d\omega, \quad [12b]$$

where

$$B_n'(\rho, z) = \frac{n+1}{\rho(\rho^2+z^2)^{n/2}} G_{n+1}^{-1/2}\left[\frac{z}{(\rho^2+z^2)^{1/2}}\right], \quad [13a]$$

$$D_n'(\rho, z) = \frac{n+1}{\rho(\rho^2+z^2)^{(n-2)/2}} G_{n+1}^{-1/2}\left[\frac{z}{(\rho^2+z^2)^{1/2}}\right] - \frac{2z}{\rho(\rho^2+z^2)^{(n-1)/2}} G_n^{-1/2}\left[\frac{z}{(\rho^2+z^2)^{1/2}}\right], \quad [13b]$$

$$B_n''(\rho, z) = \frac{1}{(\rho^2+z^2)^{(n+1)/2}} P_n\left[\frac{z}{(\rho^2+z^2)^{1/2}}\right], \quad [13c]$$

$$D_n''(\rho, z) = \frac{2}{(\rho^2+z^2)^{(n-1)/2}} G_n^{-1/2}\left[\frac{z}{(\rho^2+z^2)^{1/2}}\right] + \frac{1}{(\rho^2+z^2)^{(n-1)/2}} P_n\left[\frac{z}{(\rho^2+z^2)^{1/2}}\right], \quad [13d]$$

$$F^*(\omega, z) = [X(\omega) + zY(\omega)]\, e^{\omega z}, \quad [14a]$$

$$G^*(\omega, z) = [\omega X(\omega) + (1+\omega z) Y(\omega)]\, e^{\omega z}/\omega \quad [14b]$$

and $P_n$ is the Legendre polynomial of order $n$. For the cases of a solid plane wall and a planar free surface, [12a, b] can be simplified by using the boundary conditions [5b] and [6a, b], respectively.

*3.1. A solid plane*

Application of the no-slip condition [5b] at the solid plane to [12a, b] leads to

$$\int_0^\infty \omega J_1(\omega\rho)G^*(\omega, d)\,d\omega = \sum_{n=2}^{\infty} [B_n B_n'(\rho, d-h) + D_n D_n'(\rho, d-h)] \qquad [15a]$$

and

$$\int_0^\infty \omega J_0(\omega\rho)F^*(\omega, d)\,d\omega = -\sum_{n=2}^{\infty} [B_n B_n''(\rho, d-h) + D_n D_n''(\rho, d-h)]. \qquad [15b]$$

Inversing the above Hankel transforms and using the properties of the Legendre and Gegenbauer polynomials result in

$$F^*(\omega, d) = -\sum_{n=2}^{\infty} \frac{\omega^{n-3}}{n!} e^{-\omega(d-h)}\{B_n\omega^2 + D_n[(2n-3)\omega(d-h) - (n-1)(n-3)]\} \qquad [16a]$$

and

$$G^*(\omega, d) = -\sum_{n=2}^{\infty} \frac{\omega^{n-3}}{n!} e^{-\omega(d-h)}\{B_n\omega^2 + D_n[(2n-3)\omega(d-h) - n(n-2)]\}. \qquad [16b]$$

Utilizing [14a, b] and taking $z = d$, one can express $X(\omega)$ and $Y(\omega)$ in terms of $F^*(\omega, d)$ and $G^*(\omega, d)$:

$$X(\omega) = [(1 + \omega d)F^*(\omega, d) - \omega d G^*(\omega, d)]\, e^{-\omega d} \qquad [17a]$$

and

$$Y(\omega) = -[F^*(\omega, d) - G^*(\omega, d)]\omega\, e^{-\omega d}. \qquad [17b]$$

Substitution of [14a, b], [16a, b] and [17a, b] into [12a, b] leads to the velocity components for the fluid motion in terms of the unknown coefficients $B_n$ and $D_n$ only. After considerable algebraic manipulation, the reflection of the Sampson singularity at the point $\rho = 0$ and $z = h$ with respect to a solid plane at $z = d$ (superimposing with the singularity itself) is obtained in the form

$$\Psi = \sum_{n=2}^{\infty} [B_n\beta_n'''(\rho, z, h) + D_n\delta_n'''(\rho, z, h)], \qquad [18]$$

$$v_\rho = \sum_{n=2}^{\infty} [B_n\beta_n'(\rho, z, h) + D_n\delta_n'(\rho, z, h)] \qquad [19a]$$

and

$$v_z = \sum_{n=2}^{\infty} [B_n\beta_n''(\rho, z, h) + D_n\delta_n''(\rho, z, h)], \qquad [19b]$$

where

$$\beta_n'''(\rho, z, h) = B_n'''(\rho, z-h) - B_n'''(\rho, 2d-z-h) - 2(n+1)(d-z)B_{n+1}'''(\rho, 2d-z-h), \qquad [20a]$$

$$\delta_n'''(\rho, z, h) = D_n'''(\rho, z-h) - D_n'''(\rho, 2d-z-h) + 2(n-2)(d-z)B_{n-1}'''(\rho, 2d-z-h) - 2(2n-3)(d-h)(d-z)B_n'''(\rho, 2d-z-h), \qquad [20b]$$

$$\beta_n'(\rho, z, h) = B_n'(\rho, z-h) - B_n'(\rho, 2d-z-h) + 2(n+1)(d-z)B_{n+1}'(\rho, 2d-z-h), \qquad [21a]$$

$$\delta_n'(\rho, z, h) = D_n'(\rho, z-h) - D_n'(\rho, 2d-z-h) - (2/n)(n-1)(n-3)(d-z)B_{n-1}'(\rho, 2d-z-h) + 2(2n-3)(d-h)(d-z)B_n'(\rho, 2d-z-h), \qquad [21b]$$

$$\beta_n''(\rho, z, h) = B_n''(\rho, z-h) - B_n''(\rho, 2d-z-h) - 2(n+1)(d-z)B_{n+1}''(\rho, 2d-z-h) \qquad [21c]$$

and

$$\delta_n''(\rho, z, h) = D_n''(\rho, z-h) - D_n''(\rho, 2d-z-h) + 2(n-2)(d-z)B_{n-1}''(\rho, 2d-z-h) - 2(2n-3)(d-h)(d-z)B_n''(\rho, 2d-z-h). \quad [21d]$$

*3.2. A planar free surface*

For the case of a free surface plane, we let the velocity components in [12a, b] satisfy the boundary condition [6a, b] on the plane. This yields [15b] and

$$\int_0^\infty \omega J_1(\omega\rho)H^*(\omega, d)\,d\omega = \sum_{n=2}^{\infty} \{B_n[-(n+1)B_{n+1}'(\rho, d-h)] + D_n[-(n+1)D_{n+1}'(\rho, d-h) + 2(d-h)B_n'(\rho, d-h) - (2/n)B_{n-1}'(\rho, d-h)]\}, \quad [22]$$

where

$$H^*(\omega, z) = \frac{\partial G^*}{\partial z} = [\omega X(\omega) + (2+\omega z)Y(\omega)]\,e^{\omega z}. \quad [23]$$

Inversing the Hankel transform in [22] and using the properties of Gegenbauer polynomials lead to

$$H^*(\omega, d) = -\sum_{n=2}^{\infty} \frac{\omega^{n-2}}{n!} e^{-\omega(d-h)}\{B_n\omega^2 + D_n[(2n-3)\omega(d-h) - n^2 + 3]\}. \quad [24]$$

Using [14a] and [23] and taking $z = d$, one can express $X(\omega)$ and $Y(\omega)$ in terms of $F^*(\omega, d)$ and $H^*(\omega, d)$:

$$X(\omega) = \tfrac{1}{2}[(2+\omega d)F^*(\omega, d) - dH^*(\omega, d)]\,e^{-\omega d} \quad [25a]$$

and

$$Y(\omega) = \tfrac{1}{2}[-\omega F^*(\omega, d) + H^*(\omega, d)]\,e^{-\omega d}. \quad [25b]$$

Substitution of [16a], [24] and [25a, b] into [10] and utilization of [2a, b] lead to the stream function and velocity components for the fluid in the region $z \leqslant d$ in terms of the unknown coefficients $B_n$ and $D_n$ only. The results for the reflection of the Sampsonlet at the point $\rho = 0$ and $z = h$ with respect to a planar free surface at $z = d$ are

$$\Psi = \sum_{n=2}^{\infty} [B_n\alpha_n'''(\rho, z, h) + D_n\gamma_n'''(\rho, z, h)], \quad [26]$$

$$v_\rho = \sum_{n=2}^{\infty} [B_n\alpha_n'(\rho, z, h) + D_n\gamma_n'(\rho, z, h)] \quad [27a]$$

and

$$v_z = \sum_{n=2}^{\infty} [B_n\alpha_n''(\rho, z, h) + D_n\gamma_n''(\rho, z, h)], \quad [27b]$$

where

$$\alpha_n'''(\rho, z, h) = B_n'''(\rho, z-h) - B_n'''(\rho, 2d-z-h), \quad [28a]$$

$$\gamma_n'''(\rho, z, h) = D_n'''(\rho, z-h) - \frac{2n-3}{n}(2d-z-h)B_n'''(\rho, 2d-z-h) + \frac{n-3}{n}B_{n-2}'''(\rho, 2d-z-h), \quad [28b]$$

$$\alpha_n'(\rho, z, h) = B_n'(\rho, z-h) + B_n'(\rho, 2d-z-h), \quad [29a]$$

$$\gamma'_n(\rho, z, h) = D'_n(\rho, z-h) + \frac{2n-3}{n}(2d-z-h)B'_{n-1}(\rho, 2d-z-h)$$

$$+\frac{n-2}{n-1}B'_{n-2}(\rho, 2d-z-h), \qquad [29b]$$

$$\alpha''_n(\rho, z, h) = B''_n(\rho, z-h) - B''_n(\rho, 2d-z-h) \qquad [29c]$$

and

$$\gamma''_n(\rho, z, h) = D''_n(\rho, z-h) - \frac{2n-3}{n}(2d-z-h)B''_{n-1}(\rho, 2d-z-h)$$

$$+\frac{n-3}{n}B''_{n-2}(\rho, 2d-z-h). \qquad [29d]$$

Equations [19a, b] and [27a, b] for the velocity fields caused by a Sampsonlet in the presence of a solid plane and a free surface plane, respectively, will be utilized in the following sections to formulate the velocity field induced by the axisymmetric motion of a body of revolution toward a plane surface.

## 4. SOLUTIONS FOR THE MOTION OF A SPHERE NORMAL TO A PLANAR BOUNDARY

In this section the planar reflection of a Sampson singularity derived in the previous section is used to obtain solutions for the motion of a spherical body of radius $a$ toward an infinite plane. The results will be compared with the exact solutions obtained by Maude (1961) and Brenner (1961) using spherical bipolar coordinates.

The disturbance of the flow field produced by a sphere can be represented by a Sampsonlet placed at its center which is the origin of the coordinate frame. Thus, the velocity components for the fluid motion caused by a sphere moving perpendicular to a solid plane are given by [19a, b] with $h = 0$:

$$v_\rho = \sum_{n=2}^{\infty} [B_n\beta'_n(\rho, z, 0) + D_n\delta'_n(\rho, z, 0)] \qquad [30a]$$

and

$$v_z = \sum_{n=2}^{\infty} [B_n\beta''_n(\rho, z, 0) + D_n\delta''_n(\rho, z, 0)]. \qquad [30b]$$

To determine the unknown constants $B_n$ and $D_n$, one can apply the boundary condition [5a] at the sphere surface to these velocity components to yield

$$\sum_{n=2}^{\infty} [B_n\beta'_n(\rho, z, 0) + D_n\delta'_n(\rho, z, 0)] = 0 \qquad (\rho^2 + z^2 = a^2). \qquad [31a, b]$$

$$\sum_{n=2}^{\infty} [B_n\beta''_n(\rho, z, 0) + D_n\delta''_n(\rho, z, 0)] = U$$

Similarly, for the case of the motion of a sphere toward a planar free surface, the fluid velocity field can be obtained from [27a, b] with $h = 0$:

$$v_\rho = \sum_{n=2}^{\infty} [B_n\alpha'_n(\rho, z, 0) + D_n\gamma'_n(\rho, z, 0)] \qquad [32a]$$

and

$$v_z = \sum_{n=2}^{\infty} [B_n\alpha''_n(\rho, z, 0) + D_n\gamma''_n(\rho, z, 0)]. \qquad [32b]$$

Application of [5a] and [32a, b] leads to the equations to determine $B_n$ and $D_n$:

$$\sum_{n=2}^{\infty} [B_n \alpha_n'(\rho, z, 0) + D_n \gamma_n'(\rho, z, 0)] = 0$$

$$(\rho^2 + z^2 = a^2). \qquad [33a, b]$$

$$\sum_{n=2}^{\infty} [B_n \alpha_n''(\rho, z, 0) + D_n \gamma_n''(\rho, z, 0)] = U$$

Substituting [30a, b] (or [18]) or [32a, b] (or [26]) into [7] and applying the orthogonality properties of the Gegenbauer polynomials, one can obtain a simple formula for the drag force exerted by the fluid on the body:

$$F = 4\pi\eta D_2. \qquad [34]$$

That is, only the first multipole of the Sampson singularity contributes to the drag exerted on the body.

The exact expression for the drag force on a sphere moving perpendicular to a plane surface bounding a semi-infinite viscous fluid is given by Maude (1961) and Brenner (1961) as

$$F = -6\pi\eta a U f, \qquad [35]$$

where $f$, which is a function of the ratio of the sphere radius to the distance of the sphere center from the planar boundary, is the correction to Stokes' law arising from the presence of the plane. For the case of a solid plane wall,

$$f = \tfrac{4}{3}\sinh\xi \sum_{n=1}^{\infty} \frac{n(n+1)}{(2n-1)(2n+3)} \left[ \frac{2\sinh(2n+1)\xi + (2n+1)\sinh 2\xi}{4\sinh^2(n+\frac{1}{2})\xi - (2n+1)^2 \sinh^2 \xi} - 1 \right]; \qquad [36]$$

for the case of a free surface,

$$f = \tfrac{4}{3}\sinh\xi \sum_{n=1}^{\infty} \frac{n(n+1)}{(2n-1)(2n+3)} \left[ \frac{4\cosh^2(n+\frac{1}{2})\xi + (2n+1)^2 \sinh^2 \xi}{2\sinh(2n+1)\xi - (2n+1)\sinh 2\xi} - 1 \right]. \qquad [37]$$

In [36] and [37] the bipolar-coordinate parameter $\xi$ is related to $a/d$ via the expression

$$\xi = \operatorname{sech}^{-1} \frac{a}{d}. \qquad [38]$$

To satisfy the conditions [31a, b] or [33a, b] exactly along the entire semicircular generating arc of the sphere in a meridian plane would require the solution of the entire infinite array of unknown constants $B_n$ and $D_n$. However, the boundary collocation technique (Gluckman *et al.* 1971; Dagan *et al.* 1982) enforces the boundary conditions at a finite number of discrete points on the body's generating arc and truncates the infinite series [30a, b] or [32a, b] into finite ones. The unknown constants in each term of the series permit one to satisfy the exact boundary conditions at one discrete point on the body surface. Thus, if the boundary is approximated by satisfying conditions [31a, b] or [33a, b] at $N$ discrete points, the infinite series in [30a, b] and [32a, b] are truncated after $N$ terms, resulting in a system of $2N$ simultaneous linear algebraic equations in the truncated form of [31a, b] or [33a, b]. This matrix equation can be solved by any of the standard matrix-reduction techniques to yield the $2N$ unknown constants $B_n$ and $D_n$ required in the truncated equations of [30a, b] or [32a, b] for the flow field. The accuracy of the truncation technique can be improved to any degree by taking a sufficiently large value of $N$. Naturally, the truncation error vanishes as $N \to \infty$.

When specifying the points along the semicircular generating arc of the sphere where the boundary conditions are exactly satisfied, the first point that should be chosen is $\theta = \pi/2$, since this point defines the projected area of the sphere normal to the direction of motion. In addition, the points $\theta = 0$ and $\theta = \pi$ are important because they control the gap between the sphere and the plane. However, an examination of the system of linear algebraic equations for the unknown constants $B_n$ and $D_n$ shows that the coefficient matrix becomes singular if these points are used. To overcome the difficulty of singularity and to preserve the geometric symmetry of the spherical boundary about the equatorial plane $\theta = \pi/2$, points at $\theta = \alpha$, $\pi/2 - \alpha$, $\pi/2 + \alpha$ and $\pi - \alpha$ are taken to be four basic collocation points. Additional points along the boundary are selected as mirror-image pairs about

Table 1. Numerical results of the Stokes-law correction factor $f$ for a sphere translating perpendicular to a solid plane

| $N$ | $a/d = 0.2$ | $a/d = 0.4$ | $a/d = 0.6$ | $a/d = 0.8$ | $a/d = 0.9$ | $a/d = 0.95$ | $a/d = 0.99$ |
|---|---|---|---|---|---|---|---|
| 4 | 1.2851 | 1.7599 | 2.7448 | 7.7890 | 48.708 | 462.10 | 81262.0 |
| 8 | 1.2851 | 1.7563 | 2.6695 | 5.3145 | 11.583 | 45.828 | 5973.4 |
| 12 | | 1.7563 | 2.6695 | 5.3052 | 10.468 | 23.124 | 2328.9 |
| 16 | | | | 5.3053 | 10.439 | 20.934 | −60.01 |
| 20 | | | | 5.3053 | 10.440 | 20.573 | 58.524 |
| 24 | | | | | 10.441 | 20.568 | 86.041 |
| 28 | | | | | 10.441 | 20.574 | 54.063 |
| 32 | | | | | | 20.576 | 92.274 |
| 36 | | | | | | 20.576 | 97.172 |
| 52 | | | | | | | 100.73 |
| 68 | | | | | | | 100.88 |
| 72 | | | | | | | 100.89 |
| 76 | | | | | | | 100.89 |
| [a] | 1.2851 | 1.7563 | 2.6695 | 5.3053 | 10.441 | 20.576 | 100.89 |

[a]Exact solution (computed from [36]).

the plane $\theta = \pi/2$ to divide the $\theta$ coordinate into equal parts. The optimum value of $\alpha$ in this work is found to be 0.01°, with which the numerical results of the correction factor for Stokes' law can converge to at least four significant figures for any ratio of $a/d$ up to 0.99.

In tables 1 and 2, a number of numerical solutions of the Stokes-law correction factor for the motions of a sphere normal to a solid plane wall and to a planar free surface, respectively, are presented for various values of the spacing parameter $a/d$ using the collocation technique. A DEC 5240 work station was used to perform the calculations. All of the results were obtained by increasing the number of collocation points $N$ until the convergence of five significant digits is achieved (except for one case of $a/d = 0.99$). The exact solutions for $f$ calculated using [36] or [37] are also listed in the bottom row of tables 1 and 2 for comparison. It can be seen that the results from the collocation method agree very well with the exact results for the desired accuracy. The rate of convergence is rapid for small values of $a/d$ and deteriorates monotonically as the distance between the sphere and the planar boundary decreases. The numerical solutions for a sphere translating to a solid plane wall using boundary collocation were also presented by Ganatos *et al.* (1980) for some cases of $a/d \leqslant 0.88$.

## 5. AXISYMMETRIC MOTION OF AN ARBITRARY PROLATE BODY TOWARD A PLANAR BOUNDARY

We consider in this section the fluid motion caused by an arbitrary prolate axisymmetric body translating along its axis of symmetry and perpendicular to a plane surface. A segment between points $A(\rho = 0, z = -c_1)$ and $B(\rho = 0, z = c_2)$ is taken along the axis of revolution inside the body

Table 2. Numerical results of the Stokes-law correction factor $f$ for a sphere translating perpendicular to a planar free surface

| $N$ | $a/d = 0.2$ | $a/d = 0.4$ | $a/d = 0.6$ | $a/d = 0.8$ | $a/d = 0.9$ | $a/d = 0.95$ | $a/d = 0.99$ |
|---|---|---|---|---|---|---|---|
| 4 | 1.1756 | 1.4259 | 1.8551 | 3.3210 | 10.217 | 57.864 | 6361.9 |
| 8 | 1.1756 | 1.4242 | 1.8282 | 2.7720 | 4.4467 | 10.188 | 760.03 |
| 12 | | 1.4242 | 1.8283 | 2.7724 | 4.3331 | 7.3011 | 165.31 |
| 16 | | | 1.8283 | 2.7724 | 4.3329 | 7.1522 | 80.860 |
| 20 | | | | | 4.3330 | 7.1407 | −4.082 |
| 24 | | | | | 4.3331 | 7.1410 | 21.382 |
| 28 | | | | | 4.3331 | 7.1415 | 20.008 |
| 32 | | | | | | 7.1416 | 27.428 |
| 36 | | | | | | 7.1416 | 27.411 |
| 52 | | | | | | | 27.828 |
| 64 | | | | | | | 27.856 |
| 68 | | | | | | | 27.858 |
| 72 | | | | | | | 27.870 |
| [a] | 1.1756 | 1.4242 | 1.8283 | 2.7724 | 4.3331 | 7.1416 | 27.860 |

[a]Exact solution (computed from [37]).

on which a set of Sampson spherical singularities are distributed ($c_1$ and $c_2$ are positive constants). If the nose and the tail of the body are round, then their centers of curvature can be chosen as A and B. The general solution of the flow field outside the body in the semi-infinite fluid can be constructed by the superposition of the planar reflection of the Sampsonlets distributed on the segment AB. For the case of a solid plane wall, [19a, b] are used to result in

$$v_\rho = \sum_{n=2}^{\infty} \int_{-c_1}^{c_2} [B_n(t)\beta'_n(\rho, z, t) + D_n(t)\delta'_n(\rho, z, t)]\, dt \qquad [39a]$$

and

$$v_z = \sum_{n=2}^{\infty} \int_{-c_1}^{c_2} [B_n(t)\beta''_n(\rho, z, t) + D_n(t)\delta''_n(\rho, z, t)]\, dt. \qquad [39b]$$

Equations [39a, b] provide an exact solution for [1a, b] that satisfies [5b] and [5c] and the unknown density distribution functions for the singularities, $B_n(t)$ and $D_n(t)$, must be determined from the remaining boundary condition [5a] using the collocation technique. The drag force exerted by the fluid on the axisymmetric body is obtained by substitution of [39a, b] into [7] and the application of the orthogonality properties of the Gegenbauer polynomials, with a result similar to [34]:

$$F = 4\pi\eta \int_{-c_1}^{c_2} D_2(t)\, dt. \qquad [40]$$

The density distribution functions $B_n(t)$ and $D_n(t)$ in [39a, b] can be approximated to various orders to satisfy the boundary condition at the body surface. In this work we consider the zeroth-order, first-order and second-order approximations.

### *5.1. Constant density distribution*

In the constant density approximation, the segment AB is divided into $M$ small segments and the density distribution functions in each small segment are substituted by constants. Let $t_{m-1}$ and $t_m$ denote the coordinates of the two end points for the $m$th segment, then one has $t_0 = -c_1$ and $t_M = c_2$. If the length of each segment is the same, then $t_j = -c_1 + j(c_1 + c_2)/M$ for $j = 1, 2, \ldots, M-1$. In order to use the multipole collocation technique to satisfy the no-slip condition at the body surface, the infinite series in [39a, b] are furthermore truncated after $N$ terms. With these arrangements [39a, b] become

$$v_\rho = \sum_{m=1}^{M} \sum_{n=2}^{N+1} [B_{nm}\beta^*_{nm1}(\rho, z) + D_{nm}\delta^*_{nm1}(\rho, z)] \qquad [41a]$$

and

$$v_z = \sum_{m=1}^{M} \sum_{n=2}^{N+1} [B_{nm}\beta^{**}_{nm1}(\rho, z) + D_{nm}\delta^{**}_{nm1}(\rho, z)], \qquad [41b]$$

where the functions $\beta^*_{nm1}$, $\delta^*_{nm1}$, $\beta^{**}_{nm1}$ and $\delta^{**}_{nm1}$ are defined by [A6]–[A9] in the appendix and $B_{nm}$ and $D_{nm}$ are unknown density constants.

Application of the boundary condition [5a] to [41a, b] gives

$$\sum_{m=1}^{M} \sum_{n=2}^{N+1} [B_{nm}\beta^*_{nm1}(\rho, z) + D_{nm}\delta^*_{nm1}(\rho, z)] = 0$$
$$\sum_{m=1}^{M} \sum_{n=2}^{N+1} [B_{nm}\beta^{**}_{nm1}(\rho, z) + D_{nm}\delta^{**}_{nm1}(\rho, z)] = U \qquad \text{(on } S_b\text{)}. \qquad [42a, b]$$

The collocation method allows the body's boundary to be approximated by satisfying [42a, b] at $MN$ discrete values of $z$ (rings) on its surface. This results in a set of $2MN$ simultaneous linear algebraic equations, which can be solved by any matrix-reduction technique to yield the $2MN$ density constants $B_{nm}$ and $D_{nm}$ required in [41a, b] for the fluid velocity field. Once these constants are determined, the drag force on the body can be obtained from [40], with the result

$$F = 4\pi\eta \sum_{m=1}^{M} D_{2m}(t_m - t_{m-1}). \qquad [43]$$

*5.2. Linear density distribution*

The segment AB is divided into $M$ small segments, as we did in the previous subsection. However, the density functions in the $m$th segment are now replaced by linear functions:

$$\begin{bmatrix} B_n(t) \\ D_n(t) \end{bmatrix} = \frac{t - t_{m-1}}{t_m - t_{m-1}} \begin{bmatrix} B_{nm} \\ D_{nm} \end{bmatrix} + \frac{t_m - t}{t_m - t_{m-1}} \begin{bmatrix} B_{n(m-1)} \\ D_{n(m-1)} \end{bmatrix} \quad \text{for } t_{m-1} \leqslant t \leqslant t_m. \tag{44}$$

Here, $t_{m-1}$ and $t_m$ are the coordinates of the end points of the segment and $B_{n(m-1)}$, $D_{n(m-1)}$, $B_{nm}$ and $D_{nm}$ are the corresponding density constants at these points.

Substituting [44] into [39a, b] and truncating the infinite series after $N$ terms, one has

$$v_\rho = \sum_{m=1}^{M} \sum_{n=2}^{N+1} [B_{n(m-1)} V'_{nm1}(\rho, z) + B_{nm} V'_{nm2}(\rho, z) + D_{n(m-1)} W'_{nm1}(\rho, z) + D_{nm} W'_{nm2}(\rho, z)] \tag{45a}$$

and

$$v_z = \sum_{m=1}^{M} \sum_{n=2}^{N+1} [B_{n(m-1)} V''_{nm1}(\rho, z) + B_{nm} V''_{nm2}(\rho, z) + D_{n(m-1)} W''_{nm1}(\rho, z) + D_{nm} W''_{nm2}(\rho, z)], \tag{45b}$$

where the functions $V'_{nm1}$, $V'_{nm2}$, $W'_{nm1}$, $W'_{nm2}$, $V''_{nm1}$, $V''_{nm2}$, $W''_{nm1}$ and $W''_{nm2}$ are defined by [A1] and [A2] in the appendix. Application of the boundary condition [5a] to [45a, b] can be accomplished by utilizing the collocation technique. On the body surface, [5a] along with [45a, b] are applied at $(M + 1)N$ discrete values of $z$ (rings). This generates a set of $2(M + 1)N$ linear algebraic equations for the $2(M + 1)N$ unknown constants $B_{nm}$ and $D_{nm}$. The fluid velocity field is completely solved once these coefficients are determined.

The drag force exerted by the fluid on the body can be determined by [40] with the substitution of $D_2(t)$ expressed by [44]. The result is

$$F = 2\pi\eta \sum_{m=1}^{M} [D_{2(m-1)} + D_{2m}](t_m - t_{m-1}). \tag{46}$$

*5.3. Quadratic density distribution*

Similar to in subsections 5.1 and 5.2, the segment AB is again divided into $M$ small segments. In the quadratic density approximation, two end points and one middle point are taken to express the density distribution functions in each segment. Thus,

$$\begin{bmatrix} B_n(t) \\ D_n(t) \end{bmatrix} = \frac{(t - t_{m-1})(t - \bar{t}_m)}{(t_m - t_{m-1})(t_m - \bar{t}_m)} \begin{bmatrix} B_{n(2m)} \\ D_{n(2m)} \end{bmatrix} + \frac{(t - t_m)(t - t_{m-1})}{(\bar{t}_m - t_m)(\bar{t}_m - t_{m-1})} \begin{bmatrix} B_{n(2m-1)} \\ D_{n(2m-1)} \end{bmatrix}$$
$$+ \frac{(t - t_m)(t - \bar{t}_m)}{(t_{m-1} - t_m)(t_{m-1} - \bar{t}_m)} \begin{bmatrix} B_{n(2m-2)} \\ D_{n(2m-2)} \end{bmatrix} \quad \text{for } t_{m-1} \leqslant t \leqslant t_m. \tag{47}$$

Here $\bar{t}_m = (t_{m+1} + t_m)/2$, is the coordinate of the center of the $m$th segment, and $B_{n(2m-2)}$, $D_{n(2m-2)}$, $B_{n(2m-1)}$, $D_{n(2m-1)}$, $B_{n(2m)}$ and $D_{n(2m)}$ are the corresponding density constants at the two end points and the middle point of the segment.

Substituting [47] into [39a, b] and truncating the infinite series after $N$ terms, one obtains

$$v_\rho = \sum_{m=1}^{M} \sum_{n=2}^{N+1} [B_{n(2m-2)} V^*_{nm1}(\rho, z) + B_{n(2m-1)} V^*_{nm2}(\rho, z) + B_{n(2m)} V^*_{nm3}(\rho, z)$$
$$+ D_{n(2m-2)} W^*_{nm1}(\rho, z) + D_{n(2m-1)} W^*_{nm2}(\rho, z) + D_{n(2m)} W^*_{nm3}(\rho, z)] \tag{48a}$$

and

$$v_z = \sum_{m=1}^{M} \sum_{n=2}^{N+1} [B_{n(2m-2)} V^{**}_{nm1}(\rho, z) + B_{n(2m-1)} V^{**}_{nm2}(\rho, z) + B_{n(2m)} V^{**}_{nm3}(\rho, z)$$
$$+ D_{n(2m-2)} W^{**}_{nm1}(\rho, z) + D_{n(2m-1)} W^{**}_{nm2}(\rho, z) + D_{n(2m)} W^{**}_{nm3}(\rho, z)], \tag{48b}$$

where the functions $V^*_{nmk}$, $W^*_{nmk}$, $V^{**}_{nmk}$ and $W^{**}_{nmk}$ $(k = 1, 2, 3)$ are defined by [A3]–[A5] in the appendix. To use the collocation technique, the boundary condition [5a] after the substitution of

[48a, b] is applied at $(2M+1)N$ discrete values of $z$ (rings) along the surface of the body. The resulting system of $2(2M+1)N$ linear algebraic equations can be solved to yield the $2(2M+1)N$ unknown constants $B_{nm}$ and $D_{nm}$ required in [48a, b] for the fluid velocity components.

Substituting $D_2(t)$, given in [47], into [40], the drag force exerted on the body is obtained as

$$F = \tfrac{2}{3}\pi\eta \sum_{m=1}^{M} [D_{2(2m-2)} + 4D_{2(2m-1)} + D_{2(2m)}](t_m - t_{m-1}). \quad [49]$$

The equations derived in this section are valid for the axisymmetric motion of a prolate body normal to a solid plane wall. For the corresponding motion toward a free surface, the functions $\beta'_n$, $\delta'_n$, $\beta''_n$ and $\delta''_n$ in [39a, b] are replaced by $\alpha'_n$, $\gamma'_n$, $\alpha''_n$ and $\gamma''_n$ respectively, and the functions $\beta^*_{nmk}$, $\delta^*_{nmk}$, $\beta^{**}_{nmk}$ and $\delta^{**}_{nmk}$ in [41a, b], [42a, b], [45a, b] and [48a, b] (with the substitution of [A1]–[A5]) are replaced by $\alpha^*_{nmk}$, $\gamma^*_{nmk}$, $\alpha^{**}_{nmk}$ and $\gamma^{**}_{nmk}$ defined by [A10]–[A13], respectively. Note that, if numerical integrations are used for the evaluation of functions $\beta^*_{nmk}$, $\delta^*_{nmk}, \ldots, \gamma^{**}_{nmk}$, the accuracy and convergence behavior of the solution of drag force depends upon the precision of these numerical integrations.

## 6. SOLUTIONS FOR THE MOTION OF A PROLATE SPHEROID TOWARD A PLANAR BOUNDARY

In this section the method presented in the previous section is used to obtain the solutions for the axisymmetric motions of a prolate spheroid perpendicular to a solid plane and to a planar free surface. The surface of the prolate spheroid is represented in the circular cylindrical coordinates by

$$z(\rho) = \pm a\left[1 - \left(\frac{\rho}{b}\right)^2\right]^{1/2}, \quad [50]$$

where $a > b > 0$ and $0 \leqslant \rho \leqslant b$. For a prolate spheroid translating with a velocity $U$ along its axis of revolution in an unbounded fluid, the exact solution for the drag force exerted on the body by the fluid is (Happel & Brenner 1983):

$$F_\infty = -6\pi\eta b U f_\infty, \quad [51a]$$

with

$$f_\infty = \{\tfrac{3}{4}(\zeta^2-1)^{1/2}[(\zeta^2+1)\coth^{-1}\zeta - \zeta]\}^{-1}, \quad [51b]$$

where $\zeta = a/c$ and $c = (a^2 - b^2)^{1/2}$, which is the half distance between the two foci of the prolate spheroid.

The force acting on a spheroid moving along its axis of symmetry and normal to a plane surface can be related to its velocity by

$$F = -6\pi\eta b U f, \quad [52]$$

where the dimensionless resistance coefficient $f$ is a function of the relative separation distance of the spheroid to the boundary and the aspect ratio of the spheroid.

In section 4, collocation solutions for the axisymmetric motion of a sphere toward a plane surface were presented and shown to be in perfect agreement with the exact solutions. We now use the same collocation scheme incorporated with the method of distribution of Sampson singularities to obtain the corresponding solution for a prolate spheroid. In table 3, numerical results of the normalized resistance coefficient $f/f_\infty$ for the axisymmetric motions of a prolate spheroid toward a solid plane and a planar free surface are presented for two representative cases of the aspect ratio $a/b$ with various values of the relative separation distance $d/a$. The values of $f/f_\infty$ are computed by applying either the linear or the quadratic density distribution at each segment for different $N$ and $M$ (which shows convergence tests). For a spheroid with its aspect ratio close to unity, a constant density distribution of Sampsonlets can usually achieve good convergence behavior for the calculation of $f$. However, when the aspect ratio of the spheroid deviates further from unity, the convergence of the constant density approximation becomes poorer and higher-order approximations should be adopted. The numerical solutions of $f/f_\infty$ for the axisymmetric motion of a prolate spheroid toward a solid plane obtained by using the boundary integral method (Hsu &

Table 3. Numerical results of the normalized resistance coefficient $f/f_\infty$ for the axisymmetric motion of a prolate spheroid toward an infinite plane

| | $N$ | $M$ | $d/a = 5.0$ | $d/a = 2.0$ | $d/a = 1.5$ | $d/a = 1.1$ |
|---|---|---|---|---|---|---|
| | | | $a/b = 2$ ($f_\infty = 1.2039$), linear density distribution | | | |
| Solid plane | 3 | 3 | 1.1567 | 1.5230 | 1.8882 | 3.6496 |
| | | 4 | 1.1567 | 1.5229 | 1.8880 | 3.6468 |
| | | 5 | | 1.5229 | 1.8880 | 3.6468 |
| | [a] | | (1.16) | (1.52) | (1.89) | (3.65) |
| Free surface | 3 | 3 | 1.0998 | 1.3063 | 1.4872 | 2.1815 |
| | | 4 | 1.0997 | 1.3062 | 1.4871 | 2.1810 |
| | | 5 | 1.0997 | 1.3062 | 1.4871 | 2.1810 |
| | | | $a/b = 10$ ($f_\infty = 2.6471$), quadratic density distribution | | | |
| Solid plane | 3 | 2 | 1.0379 | 1.128 | 1.180 | 1.143 |
| | | 3 | 1.0636 | 1.182 | 1.271 | 1.509 |
| | | 4 | 1.0636 | 1.182 | 1.270 | 1.512 |
| | | 5 | | | | 1.497 |
| | [a] | | (1.07) | (1.18) | (1.27) | (1.50) |
| Free surface | 3 | 2 | 1.0174 | 1.069 | 1.085 | 1.105 |
| | | 3 | 1.0416 | 1.116 | 1.170 | 1.306 |
| | | 4 | 1.0416 | 1.116 | 1.171 | 1.282 |
| | | 5 | | | | 1.288 |

[a]Results of Hsu & Ganatos (1989).
Values in parentheses are read from the figures.

Ganatos 1989) are also presented in table 3 for comparison. It can be seen that our results from the method of Sampson singularities agree very well with the results obtained using the boundary integral method. In general, the convergence behavior of the method of Sampsonlets is quite good, except for the case of large aspect ratio and small spacing distance.

The normalized resistance coefficient $f/f_\infty$ for the axisymmetric motions of a prolate spheroid toward a solid plane and a planar free surface as a function of the aspect ratio $a/b$ for three different values of the spacing parameter $a/d$ is plotted in figure 2. It can be seen that, due to the increase of the effective particle–boundary interaction area that offers hydrodynamic resistance to the motion of the spheroid, $f/f_\infty$ increases monotonically with the decrease of $a/b$ for a given plane surface with a fixed $a/d$. Also, $f/f_\infty$ is a monotonically increasing function of $a/d$ for a given shape of spheroid. For fixed values of $a/b$ and $a/d$, as expected, a solid plane always exerts more drag on the spheroid than a free surface does.

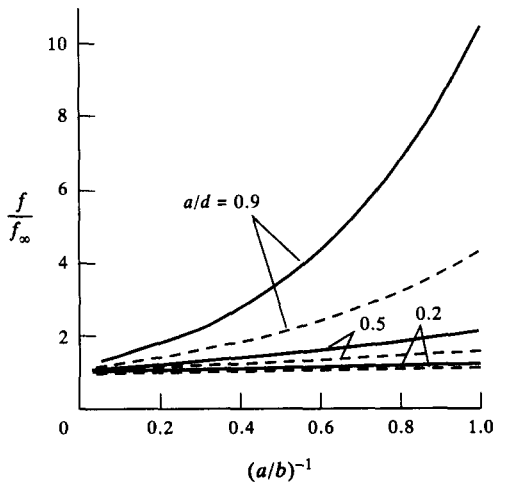


Figure 2. Plots of the normalized resistance coefficient for the axisymmetric motions of a prolate spheroid toward a solid plane (——) and a planar free surface (– – –) vs the aspect ratio of the spheroid with the ratio $a/d$ as a parameter.

Although the boundary integral method is effective and suitable for treating the motion of a body of arbitrary shape near boundaries, a severe limitation of the technique is its accuracy and the large amount of computer time required to evaluate the double integrals in the integral equations. Some of these integrals are singular and thus must be integrated analytically in the neighborhood of the singularity. For axially symmetric flow past a body of revolution as considered in the present work, the integration over the azimuthal angle $\phi$ from 0 to $2\pi$ may be performed analytically; but, a numerical integration over one coordinate is still needed for these integrals. On the other hand, when our method of distribution of Sampson singularities is used to solve for the axisymmetric flow caused by the translation of a prolate body toward a plane surface, closed-form recurrence formulas (see [A18]–[A21] in the appendix) have been derived for the integrals in [A14]–[A17], eliminating the need for a numerical integration if constant, linear or quadratic density distribution is chosen. In this way, an enormous amount of computational time has been saved and the accuracy and convergence rate of the solution can be greatly increased in comparison with the boundary integral method (Weinbaum *et al.* 1990). For example, the computation time required by solving the matrix equation for a given configuration can be approximately estimated by the formulas $T = 0.014K^2$ (for the linear density distribution) and $T = 0.035K^2$ (for the quadratic density distribution), where $T$ is the CPU time in seconds on a DEC 5240 work station and $K$ is the total number of collocation points. In contrast, the boundary integral method would need a much longer CPU time, given by the formula $T = 0.090K^2$, on an IBM 3081 computer for a similar geometry (Hsu & Ganatos 1989). Furthermore, the force and the torque on a body of revolution when its velocity disturbance is represented by the spherical singularities are known to depend only on the values of the two lowest-order coefficients associated with the spherical singularities. This observation suggests that the method of spherical singularities leads to a more accurate and efficient scheme for the resistance or mobility evaluations of the body than the boundary integral method, in which the resultant force and torque are determined by a summation of the Fourier–Legendre series after an integration over the surface of the body (Hsu & Ganatos 1989).

## 7. SOLUTIONS FOR THE MOTION OF A PROLATE CASSINI OVAL TOWARD A PLANAR BOUNDARY

In the previous section the good accuracy and convergence behavior of the method of Sampson singularities has been demonstrated by the numerical results for the axisymmetric motion of a prolate spheroid normal to a plane surface. In this section the same method is used to solve the corresponding motion of an arbitrary prolate axisymmetric body. We choose the Cassini oval as an example, because when the parameter takes different values, the oval of Cassini will have various forms, from convex contour to partial convex and partial concave contour. The surface of the prolate Cassini oval can be expressed as

$$\rho(z) = \pm[(4c^2z^2 + b^4)^{1/2} - z^2 - c^2]^{1/2}, \qquad [53]$$

where $b > c \geqslant 0$ and $0 \leqslant z \leqslant (b^2 + c^2)^{1/2}$. This body of revolution is made from the curve described by a point such that the product of its distances from two fixed points (distance $2c$ apart) is a constant $b^2$. If $(c/b)^2 \leqslant 0.5$, the surface of the prolate Cassini oval is convex everywhere and its maximum radius develops on the plane $z = 0$, as shown in figures 3(a, b). The constant $(b^2 - c^2)^{1/2}$, which is the distance from the origin to a point of intersection formed by the oval with the $\rho$-axis (taking $z = 0$), equals this maximum radius. Note that the Cassini oval degenerates to a sphere of radius $b$ when $c = 0$. If $0.5 < (c/b)^2 \leqslant 1$, as illustrated in figures 3(c, d), the surface of the body has a concave shape in the region near the plane $z = 0$ but remains convex in the other region. For this case, the maximum radius of the body which occurs at the coordinate $z = c(1 - b^4/4c^4)^{1/2}$ is equal to $b^2/2c$. For a prolate Cassini oval of any shape, the distance from its center to each of the two points on its surface intersecting the axis of symmetry is $(b^2 + c^2)^{1/2}$.

The drag force on a Cassini oval translating axisymmetrically toward a plane surface with a velocity $U$ can be written as [52], and the dimensionless resistance coefficient $f$ is a function of the separation parameter $(b^2 + c^2)^{1/2}/d$ and the aspect ratio of the body $c/b$. For the axisymmetric motion of a Cassini oval in an unbounded fluid, $f = f_\infty$, which is dependent only on $c/b$. Some values of $f_\infty$ calculated by the method of distributed Sampsonlets are tabulated in table 4. These

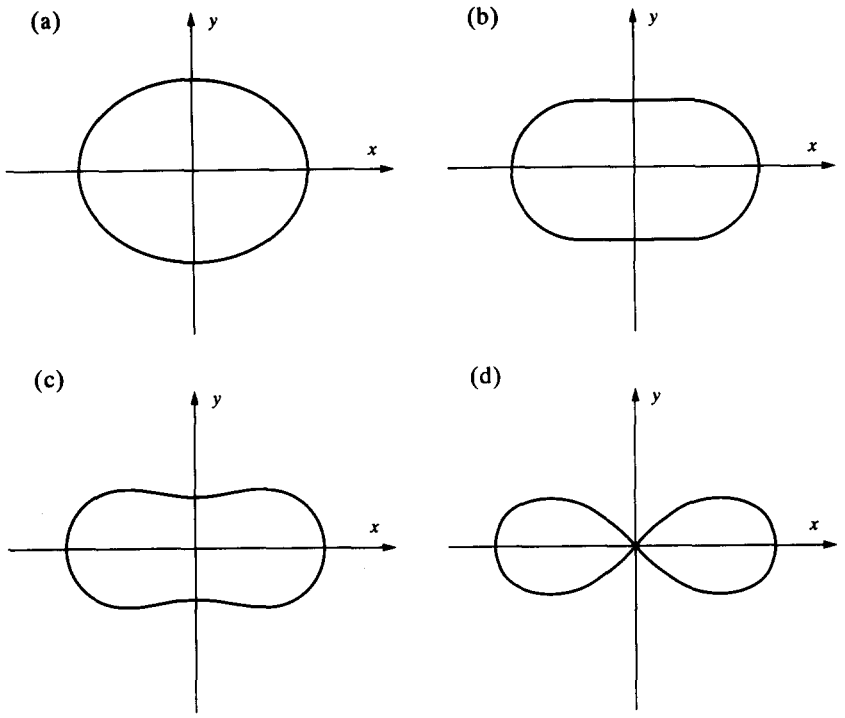


Figure 3. The various shapes of the Cassini oval with the same $b$. The coordinates $(x, y)$ denote $(z, \rho)$ for a prolate body and represent $(\rho, z)$ for an oblate body. The values of $(c/b)^2$ are: (a) 0.25; (b) 0.5; (c) 0.75; (d) 1.0.

results show that the coefficient $f_\infty$ for the movement of a prolate Cassini oval along its axis of revolution is a monotonically decreasing function of the aspect ratio $c/b$.

In figure 4 numerical results of the normalized resistance coefficient $f/f_\infty$ for the axisymmetric motions of a prolate Cassini oval normal to a planar wall and a planar free surface as a function of $c/b$ for three different values of the spacing parameter $(b^2 + c^2)^{1/2}/d$ are plotted. It can be seen that $f/f_\infty$ is a monotonically decreasing function of $c/b$ for a given plane surface with a constant $(b^2 + c^2)^{1/2}/d$. An examination of figures 3(a–d) shows why a smaller effective particle–boundary interaction area occurs for a prolate Cassini oval with a larger $c/b$ when $(b^2 + c^2)^{1/2}/d$ is fixed. Similarly to the case of a prolate spheroid considered in the previous section, $f/f_\infty$ is a monotonically increasing function of $(b^2 + c^2)^{1/2}/d$ for a given plane surface and a fixed shape of Cassini oval. Also, a solid plane always generates more viscous drag on the oval than a free surface does for given values of $c/b$ and $(b^2 + c^2)^{1/2}/d$.

Table 4. The dimensionless resistance coefficient of a Cassini oval moving along its axes of revolution in an unbounded fluid

| $(c/b)^2$ | $f_\infty$ (for prolate Cassini oval) | $f_\infty$ (for oblate Cassini oval) |
|---|---|---|
| 0 | 1.0000 | 1.0000 |
| 0.1 | 0.9700 | 1.0300 |
| 0.2 | 0.9402 | 1.0599 |
| 0.3 | 0.9107 | 1.0896 |
| 0.4 | 0.8817 | 1.1044 |
| 0.5 | 0.8534 | 1.1627 |
| 0.6 | 0.8261 | 1.1770 |
| 0.7 | 0.8002 | 1.2054 |
| 0.8 | 0.7759 | 1.2335 |
| 0.9 | 0.7537 | 1.2615 |
| 1.0 | 0.734 | 1.286 |

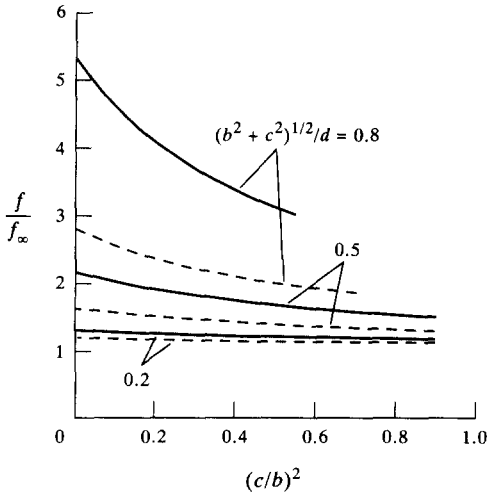


Figure 4. Plots of the normalized resistance coefficient for the axisymmetric motions of a prolate Cassini oval toward a solid plane (——) and a planar free surface (– – –) vs the aspect ratio of the Cassini oval with the ratio $(b^2 + c^2)^{1/2}/d$ as a parameter.

## 8. AXISYMMETRIC MOTION OF AN ARBITRARY OBLATE BODY TOWARD A PLANAR BOUNDARY

The axisymmetric motion of an arbitrary prolate body toward a plane surface was considered in section 5 and a set of Sampson spherical singularities must be distributed on a segment along the axis of symmetry inside the body. In this section we consider the corresponding motion of an arbitrary oblate body and the Sampsonlets should be distributed on the fundamental surface within the body. Since the oblate body and the fluid motion are axisymmetric, the fundamental surface should be a circular disk $S_d$ normal to the $z$-axis and with its center at the origin of the coordinate frame.

Let Q be an arbitrary point on $S_d$ which is expressed with the cylindrical polar coordinates $\rho = \hat{\rho}$, $\phi = \hat{\phi}$ and $z = 0$. Then the velocity disturbance at another point P($\rho = \rho$, $\phi = 0$, $z = z$) in the region $z \leqslant d$ (with an infinite solid plane situated at $z = d$) generated by the Sampson singularity at Q can be obtained using [19a, b]:

$$\hat{v}_\rho = \frac{\rho - \hat{\rho}\cos\hat{\phi}}{\rho^*} \sum_{n=2}^{\infty} [B_n\beta_n'(\rho^*, z, 0) + D_n\delta_n'(\rho^*, z, 0)], \quad [54a]$$

$$\hat{v}_\phi = \frac{\hat{\rho}\sin\hat{\phi}}{\rho^*} \sum_{n=2}^{\infty} [B_n\beta_n'(\rho^*, z, 0) + D_n\delta_n'(\rho^*, z, 0)] \quad [54b]$$

and

$$\hat{v}_z = \sum_{n=2}^{\infty} [B_n\beta_n''(\rho^*, z, 0) + D_n\delta_n''(\rho^*, z, 0)], \quad [54c]$$

where $\rho^*$ is the distance from point Q to the projection of point P on the plane $z = 0$,

$$\rho^* = (\rho^2 + \hat{\rho}^2 - 2\rho\hat{\rho}\cos\hat{\phi})^{1/2}. \quad [55]$$

Due to the axisymmetry of the fluid motion, the singularities must be distributed uniformly on the circles in $S_d$ with their centers at the origin of coordinates. Hence, the unknown density distribution coefficients $B_n$ and $D_n$ in [54a–c] are functions of $\hat{\rho}$ only.

The total disturbance of the flow field produced by the oblate body and the plane wall can be approximated by the superposition of the individual disturbances [54a–c] induced by the whole set of singularities on the fundamental disk $S_d$. Thus, at an arbitrary location in the region $z \leqslant d$, we have

$$v_\rho = \iint_{S_d} \hat{v}_\rho \, dS = \sum_{n=2}^{\infty} \int_0^{2\pi} \int_0^R \frac{\rho - \hat{\rho}\cos\hat{\phi}}{\rho^*} [B_n(\hat{\rho})\beta_n'(\rho^*, z, 0) + D_n(\hat{\rho})\delta_n'(\rho^*, z, 0)]\hat{\rho} \, d\hat{\rho} \, d\hat{\phi} \quad [56a]$$

and

$$v_z = \int\int_{S_d} \hat{v}_z \, dS = \sum_{n=2}^{\infty} \int_0^{2\pi} \int_0^R [B_n(\hat{\rho})\beta_n''(\rho^*, z, 0) + D_n(\hat{\rho})\delta_n''(\rho^*, z, 0)]\hat{\rho} \, d\hat{\rho} \, d\hat{\phi}, \quad [56b]$$

where $R$ is the radius of the disk $S_d$. The integral of $\hat{v}_\phi$ vanishes because the fluid motion is axisymmetric. Equations [56a, b] provide an exact solution for [1a, b] that satisfies [5b] and [5c] and the unknown density distribution functions $B_n(\hat{\rho})$ and $D_n(\hat{\rho})$ must be determined from the remaining boundary condition [5a] using the collocation method.

The drag force exerted by the fluid on the oblate axisymmetric body can be obtained by substituting [56a, b] into [7] and applying the orthogonality properties of the Gegenbauer polynomials. The result is

$$F = 8\pi^2\eta \int_0^R D_2(\hat{\rho})\hat{\rho} \, d\hat{\rho}. \quad [57]$$

Similar to the case of the motion of a prolate body examined in section 5, the density distribution functions $B_n(\hat{\rho})$ and $D_n(\hat{\rho})$ in [56a, b] can be approximated to various orders to satisfy the boundary condition [5a]. In order to use the boundary-collocation method, the infinite series in [56a, b] are truncated after $N$ terms. The radius of the fundamental disk $S_d$ is divided into $M$ segments, and $\hat{\rho}_{m-1}$ and $\hat{\rho}_m$ denote the radial coordinates of the inner and outer end points, respectively, for the $m$th segment. If the length of each segment is the same, then $\hat{\rho}_j = jR/M$ for $j = 0, 1, 2, \ldots,$ and $M$.

In the constant density approximation, the density distribution functions $B_n(\hat{\rho})$ and $D_n(\hat{\rho})$ in each segment are substituted by constants and the truncated form of [56a, b] can still be expressed by [41a, b] with the functions $\beta_{nm1}^*$, $\delta_{nm1}^*$, $\beta_{nm1}^{**}$ and $\delta_{nm1}^{**}$ being replaced by $E'_{nm1}$, $F'_{nm1}$, $E''_{nm1}$ and $F''_{nm1}$ defined by [A37]–[A40] in the appendix, respectively. Thus, the collocation technique described in section 5 can be used to satisfy the boundary condition [5a] and to determine the $2MN$ density constants $B_{nm}$ and $D_{nm}$ required for the fluid velocity field. Since the density functions in each segment are constant, [57] for the drag force exerted on the oblate body becomes

$$F = 4\pi^2\eta \sum_{m=1}^{M} D_{2m}(\hat{\rho}_m^2 - \hat{\rho}_{m-1}^2). \quad [58]$$

When the linear density distribution of Sampsonlets is employed, the distribution functions $B_n(\hat{\rho})$ and $D_n(\hat{\rho})$ in the $m$th segment are given by [44] with $t$, $t_{m-1}$ and $t_m$ being replaced by $\hat{\rho}$, $\hat{\rho}_{m-1}$ and $\hat{\rho}_m$, respectively. Hence, the fluid velocity components have the same form as [45a, b], but the functions $\beta_{nmk}^*$, $\delta_{nmk}^*$, $\beta_{nmk}^{**}$ and $\delta_{nmk}^{**}$ in [A1] and [A2] must be replaced by $E'_{nmk}$, $F'_{nmk}$, $E''_{nmk}$ and $F''_{nmk}$, respectively. Application of the boundary condition [5a] to these velocity components can be accomplished by using the collocation method. After determining the $2(M+1)N$ unknown constants $B_{nm}$ and $D_{nm}$, the drag force exerted on the body by the fluid can be evaluated by the formula

$$F = \tfrac{4}{3}\pi^2\eta \sum_{m=1}^{M} [(\hat{\rho}_m + 2\hat{\rho}_{m-1})D_{2(m-1)} + (2\hat{\rho}_m + \hat{\rho}_{m-1})D_{2m}](\hat{\rho}_m - \hat{\rho}_{m-1}), \quad [59]$$

which is obtained by the substitution of $D_2(\hat{\rho})$ into [57].

In the quadratic density approximation, the distribution functions $B_n(\hat{\rho})$ and $D_n(\hat{\rho})$ in the $m$th segment are given by [47] with $t$, $t_{m-1}$, $t_m$ and $\bar{t}_m$ being replaced by $\hat{\rho}$, $\hat{\rho}_{m-1}$, $\hat{\rho}_m$ and $\bar{\rho}_m$ $(=(\hat{\rho}_{m-1} + \hat{\rho}_m)/2)$, respectively, and the fluid velocity fluid can also be written in the form of [48a, b] (after the substitution of $V_{nmk}^*$, $W_{nmk}^*$, $V_{nmk}^{**}$ and $W_{nmk}^{**}$, defined by [A3]–[A5]) with $\beta_{nmk}^*$, $\delta_{nmk}^*$, $\beta_{nmk}^{**}$ and $\delta_{nmk}^{**}$ being replaced by $E'_{nmk}$, $F'_{nmk}$, $E''_{nmk}$ and $F''_{nmk}$, respectively. To apply the boundary condition [5a] to determine the $2(2M+1)N$ unknown constants $B_{nm}$ and $D_{nm}$ required for the velocity field, the collocation technique must be used. Substituting $D_2(\hat{\rho})$ into [57], one obtains the drag force on the body as

$$F = \tfrac{4}{3}\pi^2\eta \sum_{m=1}^{M} [\hat{\rho}_{m-1}D_{2(2m-2)} + 2(\hat{\rho}_m + \hat{\rho}_{m-1})D_{2(2m-1)} + \hat{\rho}_m D_{2(2m)}](\hat{\rho}_m - \hat{\rho}_{m-1}). \quad [60]$$

Up to this point, the analysis in this section is valid for the axisymmetric motion of an oblate body perpendicular to a soid plane wall. For the corresponding motion toward a free surface, the functions $\beta'_n$, $\delta'_n$, $\beta''_n$ and $\delta''_n$ in [54a–c] and [56a, b] are replaced by $\alpha'_n$, $\gamma'_n$, $\alpha''_n$ and $\gamma''_n$, respectively. Thus, the functions $E'_{nmk}$, $F'_{nmk}$, $E''_{nmk}$ and $F''_{nmk}$ in the analysis must be replaced by $G'_{nmk}$, $H'_{nmk}$, $G''_{nmk}$ and $H''_{nmk}$, defined by [A41]–[A44], respectively. To evaluate functions $E'_{nmk}$, $F'_{nmk}, \ldots, H''_{nmk}$, numerical integrations are required.

## 9. SOLUTIONS FOR THE MOTION OF AN OBLATE SPHEROID TOWARD A PLANAR BOUNDARY

In section 6, numerical solutions of the drag force experienced by a prolate spheroid translating axisymmetrically toward a plane surface were presented. In this section the similar singularity method and collocation technique described in the previous section will be used to solve the corresponding motion of an oblate spheroid. The shape of the oblate spheroid can still be represented by [50], but now with $b > a > 0$. In addition, the exact solution for the drag force exerted on an oblate spheroid moving with a velocity $U$ along its axis of symmetry in an unbounded fluid can be expressed as [51a], with the coefficient $f_\infty$ given by (Happel & Brenner 1983):

$$f_\infty = \{\tfrac{3}{4}(\zeta^2+1)^{1/2}[\zeta - (\zeta^2-1)\cot^{-1}\zeta]\}^{-1}, \qquad [61]$$

where $\zeta = a/c$ and $c = (b^2 - a^2)^{1/2}$, which is the radius of the focal circle of the oblate spheroid. Again we employ [52] to define the dimensionless resistance coefficient $f$ for the axisymmetric motion of an oblate spheroid toward a plane surface.

The numerical solutions of $f/f_\infty$ for the axisymmetric motions of an oblate spheroid toward a solid plane and a planar free surface are presented in table 5 for two representative cases of the aspect ratio $a/b$ with various values of the relative separation $d/b$. Either the linear or the quadratic density approximation is used to calculate the values of $f/f_\infty$ and to show the convergence tests. The numerical results for the motion of an oblate spheroid along its axis of revolution and normal to a solid plane obtained using the boundary integral method (Hsu & Ganatos 1989) are also listed in table 5 for comparison. Similarly to the case of a prolate spheroid considered in section 6, the convergence behavior of the method of Sampson singularities in general is satisfactory. The

Table 5. Numerical results of the normalized resistance coefficient $f/f_\infty$ for the axisymmetric motion of an oblate spheroid toward an infinite plane

| | $N$ | $M$ | $d/b = 5.0$ | $d/b = 2.0$ | $d/b = 1.5$ | $d/b = 1.1$ | $d/b = 0.8$ | $d/b = 0.55$ |
|---|---|---|---|---|---|---|---|---|
| | | | $a/b = 0.5$ ($f_\infty = 0.90531$), linear density distribution | | | | | |
| | 5 | 4 | 1.2488 | 1.8669 | 2.1651 | 3.4129 | 9.0577 | 62.10 |
| Solid | 6 | | 1.2498 | 1.8573 | 2.3847 | 3.6468 | 7.2612 | 62.39 |
| plane | 7 | | 1.2498 | 1.8573 | 2.3852 | 3.6468 | 7.2611 | 62.51 |
| | 8 | | | | | | 7.2612 | 62.38 |
| | | [a] | (1.25) | (1.86) | 2.385 | 3.589 | 7.262 | 62.9 |
| | 5 | 4 | 1.1552 | 1.5019 | 1.7778 | 2.2608 | 3.4567 | 18.65 |
| Free | 6 | | 1.1553 | 1.4757 | 1.7175 | 2.2041 | 3.4635 | 18.51 |
| surface | 7 | | 1.1553 | 1.4757 | 1.7174 | 2.2042 | 3.4636 | 18.41 |
| | 8 | | | | 1.7174 | 2.2041 | 3.4635 | 18.53 |
| | | | $a/b = 0.1$ ($f_\infty = 0.85245$), quadratic density distribution | | | | | |
| | 4 | 2 | 1.231 | 1.749 | 2.140 | 2.866 | — | — |
| Solid | 4 | 3 | 1.231 | 1.749 | 2.141 | 2.871 | — | — |
| plane | 6 | 3 | 1.231 | 1.748 | 2.141 | 2.880 | — | — |
| | | [a] | (1.43) | (1.75) | (2.14) | (2.88) | | |
| | 4 | 2 | 1.145 | 1.426 | 1.616 | 1.941 | — | — |
| Free surface | 4 | 3 | 1.145 | 1.426 | 1.616 | 1.942 | — | — |
| | 6 | 3 | 1.145 | 1.425 | 1.615 | 1.949 | — | — |

[a]Results of Hsu & Ganatos (1989).
Values in parentheses are read from the figures.

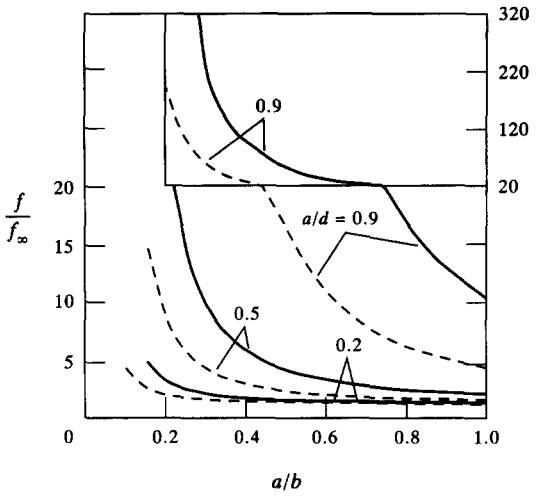


Figure 5. Plots of the normalized resistance coefficient for the axisymmetric motions of an oblate spheroid toward a solid plane (——) and a planar free surface (– – –) vs the aspect ratio of the spheroid with the ratio $a/d$ as a parameter.

agreement between our results and the boundary integral solutions is quite good, except for one case with $a/b = 0.1$ and $d/b = 5.0$ [for which the drag result of Hsu & Ganatos (1989) is obviously in error].

In figure 5, the normalized resistance coefficient $f/f_\infty$ for the axisymmetric motions of an oblate spheroid toward a solid plane and a planar free surface as a function of the aspect ratio $a/b$ for three different values of the spacing parameter $a/d$ is plotted. Similarly to the boundary effects on the motion of a prolate spheroid, $f/f_\infty$ increases montonically as the ratio $a/b$ decreases or $a/d$ increases, keeping other factors fixed. The hydrodynamic drag on the spheroid can be very large when $a/b$ is small and $a/d$ approaches unity. Again, a solid plane always exerts more drag on the oblate spheroid than a free surfae does for a given spheroid with the same separation distance to the plane.

## 10. SOLUTIONS FOR THE MOTION OF AN OBLATE CASSINI OVAL TOWARD A PLANAR BOUNDARY

In this section the method of Sampson spherical singularities is used to obtain the solutions for the axisymmetric motion of an oblate Cassini oval perpendicular to a plane surface. Of course, the same method can be utilized to solve the corresponding problem for an arbitrary oblate axisymmetric body. The surface of the oblate Cassini oval is represented by

$$z(\rho) = \pm[(4c^2\rho^2 + b^4)^{1/2} - \rho^2 - c^2]^{1/2}, \qquad [62]$$

where $b > c \geqslant 0$ and $0 \leqslant \rho \leqslant (b^2 + c^2)^{1/2}$. When $(c/b)^2 \leqslant 0.5$, the surface of the oblate Cassini oval is convex everywhere and its maximum thickness develops along the axis of revolution, as illustrated in figures 3(a, b). The constant $(b^2 - c^2)^{1/2}$, which is the distance from the origin to the point of intersection formed by the oval with the $z$-axis, equals one-half of this maximum thickness. When $0.5 < (c/b)^2 \leqslant 1$, the surface of the body has a concave shape in the region near the axis of symmetry but remains convex in the other region, as shown in figures 3(c, d). In this case, the maximum thickness of the body occurs at the coordinate $\rho = c(1 - b^4/4c^4)^{1/2}$ and one-half of this maximum thickness is equal to $b^2/2c$.

The drag force on an oblate Cassini oval moving axisymmetrically toward a plane surface with a velocity $U$ can still be written as [52] and the dimensionless resistance coefficient $f$ is a function of the aspect ratio $c/b$ and the separation parameter $a^*/d$, where $a^* = (b^2 - c^2)^{1/2}$ if $(c/b)^2 \leqslant 0.5$ and $a^* = b^2/2c$ if $(c/b)^2 > 0.5$. For the axially symmetric motion of an oblate Cassini oval in an unbounded fluid $f = f_\infty$, which is dependent on $c/b$ only. Some values of this $f_\infty$ computed by the method of Sampson singularities are also presented in table 4. Contrary to the case of a prolate

Cassini oval, the coefficient $f_\infty$ for the translation of an oblate Cassini oval along its axis of symmetry is a monotonically increasing function of $c/b$.

The normalized resistance coefficient $f/f_\infty$ for the axisymmetric motions of an oblate Cassini oval toward a solid plane and free surface plane as a function of $c/b$ for three different values of the spacing parameter $a^*/d$ is plotted in figure 6. Opposite to the situation with a prolate Cassini oval, $f/f_\infty$ for an oblate oval increases monotonically with the increase of $c/b$ for a given plane surface with a fixed $a^*/d$. This behavior can also be understood by a careful examination of figures 3(a–d). Again, $f/f_\infty$ is a monotonically increasing function of $a^*/d$ for a given plane and a given oval, and a solid plane always exerts more drag on the oval than a free surface does for fixed values of $c/b$ and $a^*/d$.

## 11. CONCLUDING REMARKS

In this work the slow motion of an arbitrary axisymmetric body in viscous fluid along its axis of revolution and perpendicular to an infinite plane has been analyzed by the use of the method of internal singularity distributions combined with the bounded-flow collocation technique. For the case of the axisymmetric motion of a prolate body, a truncated set of Sampson singularities is distributed either discretely or continuously along the axis; while for the case of an oblate body, the Sampsonlets are placed on the fundamental plane of the body. The results for the hydrodynamic drag exerted on the body indicate that the solution procedure converges rapidly and accurate solutions can be obtained for various cases of the body shape and the separation between the body and the plane. Although the numerical solutions were presented in the previous sections only for a sphere, a spheroid and a Cassini oval, the combined analytic and numerical technique utilized in this work can easily provide the hydrodynamic calculations for an axisymmetric body of other shapes.

Throughout this work we have only considered the translation of a body axisymmetrically towards a planar surface. However, the method of internal distribution of spherical singularities can easily be employed to analyze the axisymmetric rotation of an arbitrary body of revolution in the presence of an infinite planar surface. For example, the numerical solutions for the Stokes flow generated by the rotation of a prolate spheroid about its axis of symmetry which is perpendicular to a solid plane or a planar free surface were obtained by Yan *et al.* (1988) using the method of spherical singularities combined with the boundary collocation technique. Moreover,

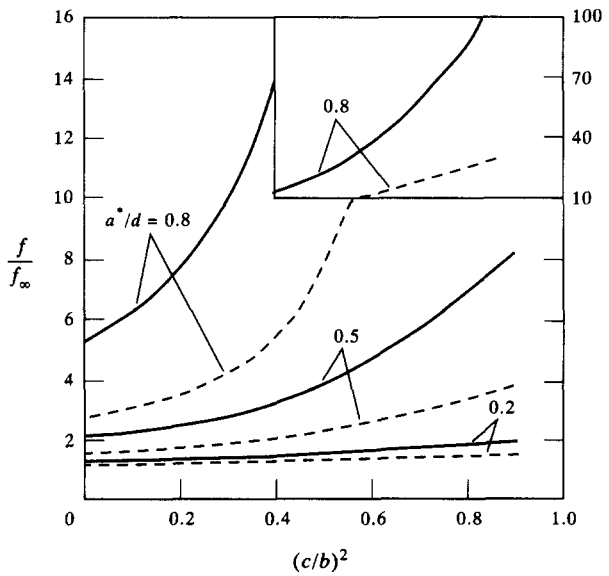


Figure 6. Plots of the normalized resistance coefficient for the axisymmetric motions of an oblate Cassini oval toward a solid plane (——) and a planar free surface (– – –) vs the aspect ratio of the Cassini oval with the ratio $a^*/d$ as a parameter, where $a^* = (b^2 - c^2)^{1/2}$ if $(c/b)^2 \leqslant 0.5$ and $a^* = b^2/2c$ if $(c/b)^2 > 0.5$.

the axisymmetric singularity distribution method can also be utilized to investigate some restricted three-dimensional (asymmetric) flows induced by the motion of a body of revolution, such as the translation of a prolate spheroid or a prolate Cassini oval in an arbitrary direction with respect to its axis of symmetry in an unbounded fluid (Lin & Wu 1986).

It is generally recognized that the distributed internal singularity methods are more limited in their range of application than the boundary integral equation method, which is much more flexible in treating problems with complicate body shapes and boundaries. Nonetheless, the singularity method presented herein has several advantages: (a) no singular integrals appear, since the collocation points lie on the body surface and the singular points lie within; (b) closed-form recurrence formulas for the integrals in the linear algebraic equations have been obtained for the case of an arbitrary prolate axisymmetric body, eliminating the need for a numerical integration; and (c) the method, when it can be used, has proved to be far more accurate and efficient than the boundary integral equation technique.

*Acknowledgements*—This research was partially supported by the National Science Council of the Republic of China. The authors thank Mr. L. C. Lien for the help with some mathematical work.

## REFERENCES

BATCHELOR, G. K. 1970 Slender-body theory for particles of arbitrary cross-section in Stokes flow. *J. Fluid Mech.* **44,** 419–440.

BRENNER, H. 1961 The slow motion of a sphere through a viscous fluid towards a plane surface. *Chem. Engng Sci.* **16,** 242–251.

CHWANG, A. T. & WU, T. Y. 1975 Hydrodynamic of low-Reynolds-number flow. Part 2. Singularity method for Stokes flows. *J. Fluid Mech.* **67,** 787–815.

COX, R. G. 1970 The motion of long slender bodies in a viscous fluid. Part 1. General theory. *J. Fluid Mech.* **44,** 791–810.

DABROS, T. 1985 A singularity method for calculating hydrodynamic forces and particle velocities in low-Reynolds-number flows. *J. Fluid Mech.* **156,** 1–21.

DAGAN, Z., PFEFFER, R. & WEINBAUM, S. 1982 Axisymmetric stagnation flow of a spherical particle near a finite planar surface at zero Reynolds number. *J. Fluid Mech.* **122,** 273–294.

GANATOS, P., PFEFFER, R. & WEINBAUM, S. 1980 A strong interaction theory for the creeping motion of a sphere between plane parallel boundaries. Part 1. Perpendicular motion. *J. Fluid Mech.* **99,** 739–753.

GLUCKMAN, M. J., PFEFFER, R. & WEINBAUM, S. 1971 A new technique for treating multi-particle slow viscous flow: axisymmetric flow past spheres and spheroids. *J. Fluid Mech.* **50,** 705–740.

GLUCKMAN, M. J., WEINBAUM, S. & PFEFFER, R. 1972 Axisymmetric slow viscous flow past an arbitrary convex body of revolution. *J. Fluid Mech.* **55,** 677–709.

GOREN, S. L. & O'NEILL, M. E. 1980 Asymmetric creeping motion of an open torus. *J. Fluid Mech.* **101,** 97–110.

HABERMAN, W. L. & SAYRE, R. M. 1958 Motion of rigid and fluid spheres in stationary and moving liquids inside cylindrical tubes. David Taylor Model Basin Report No. 1143, U.S. Navy Dept, Washington, DC.

HAPPEL, J. & BRENNER, H. 1983 *Low Reynolds Number Hydrodynamics.* Nijhoff, The Hague, The Netherlands.

HSU, R. & GANATOS, P. 1989 The motion of a rigid body in viscous fluid bounded by a plane wall. *J. Fluid Mech.* **207,** 29–72.

JEFFREY, D. J. & ONISHI, Y. 1981 The slow motion of a cylinder next to a plane wall. *Q. J. Mech. Appl. Math.* **34,** 129–137.

KEH, H. J., HORNG, K. D. & KUO, J. 1991 Boundary effects on electrophoresis of colloidal cylinders. *J. Fluid Mech.* **231,** 211–228.

KIM, S. & KARRILA, S. J. 1991 *Microhydrodynamics: Principles and Selected Applications.* Butterworth-Heinemann, Boston, MA.

LEE, S. H. & LEAL, L. G. 1982 The motion of a sphere in the presence of a deformable interface—II. A numerical study of the translation of a sphere normal to an interface. *J. Colloid Interface Sci.* **87,** 81–106.

LIN, S. & WU, W. 1986 The semi-analytic semi-numerical method to treat the three-dimension Stokes flow. *Acta Aerodyn. Sin.* **4,** 140–149 (In Chinese).

MAUDE, A. D. 1961 End effects in a falling-sphere viscometer. *Br. J. Appl. Phys.* **12,** 293–295.

OBERBECK, A. 1876 Uber stationare Flussigkeitsbewegungen mit Berucksichtigung der inner Reibung. *J. Reine Angew. Math.* **81,** 62–80.

O'NEILL, M. E. 1964 A slow motion of viscous liquid caused by a slowly moving solid sphere. *Mathematica* **11,** 67–74.

PAYNE, L. E. & PELL, W. H. 1960 The Stokes flow problem for a class of axially symmetric bodies. *J. Fluid Mech.* **7,** 529–549.

POZRIKIDIS, C. 1992 *Boundary Integral and Singularity Methods for Linearized Viscous Flow.* Cambridge Univ. Press, Cambridge, U.K.

SAMPSON, R. A. 1891 On Stokes's current function. *Phil. Trans. R. Soc.* **A182,** 449–518.

STOKES, G. G. 1851 On the effect of the internal friction of fluid on pendulums. *Trans. Camb. Phil. Soc.* **9,** 8–106.

WEINBAUM, S., GANATOS, P. & YAN, Z. 1990 Numerical multipole and boundary integral equation techniques in Stokes flow. *A. Rev. Fluid Mech.* **22,** 275–316.

WU, W. 1984 A new approach of treating the Stokes flow of nonslender prolate arbitrary axisymmetrical body. *Sci. Sin. Ser. A* **27,** 731–744.

YAN, Z., WEINBAUM, S., GANATOS, P. & PFEFFER, R. 1987 The three-dimensional hydrodynamic interaction of a finite sphere with a circular orifice at low Reynolds number. *J. Fluid Mech.* **174,** 39–68.

YAN, Z., ZHAO, Y. & LIU, W. 1988 The Stokes flow induced by the rotation of a prolate axisymmetric body in the presence of an infinite planar boundary. In *Computational Methods in Flow Analysis* (Edited by NIKI, H. & KAWAHARA, M.), Vol. 1, pp. 243–248. Okayama Univ. Sci., Okayama, Japan.

YOUNGREN, G. K. & ACRIVOS, A. 1975 Stokes flow past a particle of arbitrary shape: a numerical method of solution. *J. Fluid Mech.* **69,** 377–403.

YUAN, F. & WU, W. 1987 The Stokes flow of an arbitrary prolate axisymmetric body towards an infinite plane wall. *Appl. Math. Mech. SUT, Shanghai, China* **8,** 17–30.

ZHU, M. & WU, W. 1985 The method of continuous distribution of singularities to treat the Stokes flow of the arbitrary oblate axisymmetrical body. *Appl. Math. Mech. SUT, Shanghai, China* **6,** 929–942.

## APPENDIX

For conciseness, the definitions of some functions in sections 5 and 8 are listed in this appendix. The functions appearing in [45a, b] and [48a, b] are defined as

$$\begin{bmatrix} V'_{nm1}(\rho,z) \\ W'_{nm1}(\rho,z) \\ V''_{nm1}(\rho,z) \\ W''_{nm1}(\rho,z) \end{bmatrix} = \frac{1}{t_m - t_{m-1}} \left\{ t_m \begin{bmatrix} \beta^*_{nm1}(\rho,z) \\ \delta^*_{nm1}(\rho,z) \\ \beta^{**}_{nm1}(\rho,z) \\ \delta^{**}_{nm1}(\rho,z) \end{bmatrix} - \begin{bmatrix} \beta^*_{nm2}(\rho,z) \\ \delta^*_{nm2}(\rho,z) \\ \beta^{**}_{nm2}(\rho,z) \\ \delta^{**}_{nm2}(\rho,z) \end{bmatrix} \right\}, \quad [A1]$$

$$\begin{bmatrix} V'_{nm2}(\rho,z) \\ W'_{nm2}(\rho,z) \\ V''_{nm2}(\rho,z) \\ W''_{nm2}(\rho,z) \end{bmatrix} = \frac{-1}{t_m - t_{m-1}} \left\{ t_{m-1} \begin{bmatrix} \beta^*_{nm1}(\rho,z) \\ \delta^*_{nm1}(\rho,z) \\ \beta^{**}_{nm1}(\rho,z) \\ \delta^{**}_{nm1}(\rho,z) \end{bmatrix} - \begin{bmatrix} \beta^*_{nm2}(\rho,z) \\ \delta^*_{nm2}(\rho,z) \\ \beta^{**}_{nm2}(\rho,z) \\ \delta^{**}_{nm2}(\rho,z) \end{bmatrix} \right\}, \quad [A2]$$

$$\begin{bmatrix} V^*_{nm1}(\rho,z) \\ W^*_{nm1}(\rho,z) \\ V^{**}_{nm1}(\rho,z) \\ W^{**}_{nm1}(\rho,z) \end{bmatrix} = \frac{2}{(t_m - t_{m-1})^2}\left\{ t_m \bar{t}_m \begin{bmatrix} \beta^*_{nm1}(\rho,z) \\ \delta^*_{nm1}(\rho,z) \\ \beta^{**}_{nm1}(\rho,z) \\ \delta^{**}_{nm1}(\rho,z) \end{bmatrix} - (t_m + \bar{t}_m) \begin{bmatrix} \beta^*_{nm2}(\rho,z) \\ \delta^*_{nm2}(\rho,z) \\ \beta^{**}_{nm2}(\rho,z) \\ \delta^{**}_{nm2}(\rho,z) \end{bmatrix} + \begin{bmatrix} \beta^*_{nm3}(\rho,z) \\ \delta^*_{nm3}(\rho,z) \\ \beta^{**}_{nm3}(\rho,z) \\ \delta^{**}_{nm3}(\rho,z) \end{bmatrix} \right\}, \tag{A3}$$

$$\begin{bmatrix} V^*_{nm2}(\rho,z) \\ W^*_{nm2}(\rho,z) \\ V^{**}_{nm2}(\rho,z) \\ W^{**}_{nm2}(\rho,z) \end{bmatrix} = \frac{-4}{(t_m - t_{m-1})^2}\left\{ t_m t_{m-1} \begin{bmatrix} \beta^*_{nm1}(\rho,z) \\ \delta^*_{nm1}(\rho,z) \\ \beta^{**}_{nm1}(\rho,z) \\ \delta^{**}_{nm1}(\rho,z) \end{bmatrix} - (t_m + t_{m-1}) \begin{bmatrix} \beta^*_{nm2}(\rho,z) \\ \delta^*_{nm2}(\rho,z) \\ \beta^{**}_{nm2}(\rho,z) \\ \delta^{**}_{nm2}(\rho,z) \end{bmatrix} + \begin{bmatrix} \beta^*_{nm3}(\rho,z) \\ \delta^*_{nm3}(\rho,z) \\ \beta^{**}_{nm3}(\rho,z) \\ \delta^{**}_{nm3}(\rho,z) \end{bmatrix} \right\}, \tag{A4}$$

and

$$\begin{bmatrix} V^*_{nm3}(\rho,z) \\ W^*_{nm3}(\rho,z) \\ V^{**}_{nm3}(\rho,z) \\ W^{**}_{nm3}(\rho,z) \end{bmatrix} = \frac{2}{(t_m - t_{m-1})^2}\left\{ t_{m-1} \bar{t}_m \begin{bmatrix} \beta^*_{nm1}(\rho,z) \\ \delta^*_{nm1}(\rho,z) \\ \beta^{**}_{nm1}(\rho,z) \\ \delta^{**}_{nm1}(\rho,z) \end{bmatrix} - (t_{m-1} + \bar{t}_m) \begin{bmatrix} \beta^*_{nm2}(\rho,z) \\ \delta^*_{nm2}(\rho,z) \\ \beta^{**}_{nm2}(\rho,z) \\ \delta^{**}_{nm2}(\rho,z) \end{bmatrix} + \begin{bmatrix} \beta^*_{nm3}(\rho,z) \\ \delta^*_{nm3}(\rho,z) \\ \beta^{**}_{nm3}(\rho,z) \\ \delta^{**}_{nm3}(\rho,z) \end{bmatrix} \right\}, \tag{A5}$$

where $n = 2, 3, \ldots, N+1$ and $m = 1, 2, 3, \ldots, M$. In [41a, b], [42a, b] and [A1]–[A5],

$$\begin{aligned} \beta^*_{nmk}(\rho,z) &= \int_{t_{m-1}}^{t_m} t^{k-1} \beta'_n(\rho,z,t)\,\mathrm{d}t \\ &= B^*_{nmk}(\rho,z) - B^*_{nmk}(\rho,2d-z) + 2(n+1)(d-z)B^*_{(n+1)mk}(\rho,2d-z), \end{aligned} \tag{A6}$$

$$\begin{aligned} \delta^*_{nmk}(\rho,z) &= \int_{t_{m-1}}^{t_m} t^{k-1} \delta'_n(\rho,z,t)\,\mathrm{d}t \\ &= D^*_{nmk}(\rho,z) - D^*_{nmk}(\rho,2d-z) - (2/n)(n-1)(n-3)(d-z)B^*_{(n-1)mk}(\rho,2d-z) \\ &\quad + 2(2n-3)(d-z)[dB^*_{nmk}(\rho,2d-z) - B^*_{nm(k+1)}(\rho,2d-z)], \end{aligned} \tag{A7}$$

$$\begin{aligned} \beta^{**}_{nmk}(\rho,z) &= \int_{t_{m-1}}^{t_m} t^{k-1} \beta''_n(\rho,z,t)\,\mathrm{d}t \\ &= B^{**}_{nmk}(\rho,z) - B^{**}_{nmk}(\rho,2d-z) - 2(n+1)(d-z)B^{**}_{(n+1)mk}(\rho,2d-z) \end{aligned} \tag{A8}$$

and

$$\begin{aligned} \delta^{**}_{nmk}(\rho,z) &= \int_{t_{m-1}}^{t_m} t^{k-1} \delta''_n(\rho,z,t)\,\mathrm{d}t \\ &= D^{**}_{nmk}(\rho,z) - D^{**}_{nmk}(\rho,2d-z) + 2(n-2)(d-z)B^{**}_{(n-1)mk}(\rho,2d-z) \\ &\quad - 2(2n-3)(d-z)[dB^{**}_{nmk}(\rho,2d-z) - B^{**}_{nm(k+1)}(\rho,2d-z)], \end{aligned} \tag{A9}$$

where $k = 1, 2, 3$. Also, when the fucntions $\beta'_n$, $\delta'_n$, $\beta''_n$ and $\delta''_n$ (defined by [21a–d]) in [A6]–[A9] are replaced by $\alpha'_n$, $\gamma'_n$, $\alpha''_n$ and $\gamma'_n$ (defined by [29a–d]), respectively, one has

$$\alpha^*_{nmk}(\rho, z) = \int_{t_{m-1}}^{t_m} t^{k-1}\alpha'_n(\rho, z, t)\,dt$$

$$= B^*_{nmk}(\rho, z) + B^*_{nmk}(\rho, 2d - z), \qquad [A10]$$

$$\gamma^*_{nmk}(\rho, z) = \int_{t_{m-1}}^{t_m} t^{k-1}\gamma'_n(\rho, z, t)\,dt$$

$$= D^*_{nmk}(\rho, z) + \frac{2n-3}{n}\left[(2d - z)B^*_{(n-1)mk}(\rho, 2d - z) - B^*_{(n-1)m(k+1)}(\rho, 2d - z)\right]$$

$$- \frac{n-2}{n-1}B^*_{(n-2)mk}(\rho, 2d - z), \qquad [A11]$$

$$\alpha^{**}_{nmk}(\rho, z) = \int_{t_{m-1}}^{t_m} t^{k-1}\alpha''_n(\rho, z, t)\,dt$$

$$= B^{**}_{nmk}(\rho, z) - B^{**}_{nmk}(\rho, 2d - z) \qquad [A12]$$

and

$$\gamma^{**}_{nmk}(\rho, z) = \int_{t_{m-1}}^{t_m} t^{k-1}\gamma''_n(\rho, z, t)\,dt$$

$$= D^{**}_{nmk}(\rho, z) - \frac{2n-3}{n}\left[(2d - z]B^{**}_{(n-1)mk}(\rho, 2d - z) - B^{**}_{(n-1)m(k+1)}(\rho, 2d - z)\right]$$

$$+ \frac{n-3}{n}B^{**}_{(n-2)mk}(\rho, 2d - z). \qquad [A13]$$

In [A6]–[A13],

$$B^*_{nmk}(\rho, z) = \int_{t_{m-1}}^{t_m} t^{k-1}B'_n(\rho, z - t)\,dt, \qquad [A14]$$

$$D^*_{nmk}(\rho, z) = \int_{t_{m-1}}^{t_m} t^{k-1}D'_n(\rho, z - t)\,dt, \qquad [A15]$$

$$B^{**}_{nmk}(\rho, z) = \int_{t_{m-1}}^{t_m} t^{k-1}B''_n(\rho, z - t)\,dt, \qquad [A16]$$

and

$$D^{**}_{nmk}(\rho, z) = \int_{t_{m-1}}^{t_m} t^{k-1}D''_n(\rho, z - t)\,dt, \qquad [A17]$$

where $k = 1, 2, 3, 4$. The above four integrals can be evaluated analytically using [13a–d] for the definitions of functions $B'_n$, $D'_n$, $B''_n$ and $D''_n$; the results are expressed recurrently as

$$B^*_{nmk}(\rho, z) = t_m^{k-1}R'_n(\rho, z - t_m) - t_{m-1}^{k-1}R'_n(\rho, z - t_{m-1}) - \frac{k-1}{n}B^*_{(n-1)m(k-1)}(\rho, z) \quad (n \geqslant 1), \qquad [A18]$$

$$D^*_{nmk}(\rho, z) = t_m^{k-1}S'_n(\rho, z - t_m) - t_{m-1}^{k-1}S'_n(\rho, z - t_{m-1}) - \frac{k-1}{n}D^*_{(n-1)m(k-1)}(\rho, z)$$

$$+ \frac{2(k-1)}{n(n-1)}\left[B^*_{(n-2)mk}(\rho, z) - zB^*_{(n-2)m(k-1)}(\rho, z)\right] \quad (n \geqslant 2), \qquad [A19]$$

$$B^{**}_{nmk}(\rho, z) = t_m^{k-1}R''_n(\rho, z - t_m) - t_{m-1}^{k-1}R''_n(\rho, z - t_{m-1}) - \frac{k-1}{n}B^{**}_{(n-1)m(k-1)}(\rho, z) \quad (n \geqslant 1), \qquad [A20]$$

and

$$D^{**}_{nmk}(\rho,z)=t_m^{k-1}S''_n(\rho,z-t_m)-t_{m-1}^{k-1}S''_n(\rho,z-t_{m-1})-\frac{k-1}{n}D^{**}_{(n-1)m(k-1)}(\rho,z)$$
$$+\frac{2(k-1)}{n(n-1)}[B^{**}_{(n-2)mk}(\rho,z)-zB^{**}_{(n-2)m(k-1)}(\rho,z)$$
$$-\frac{1}{n-2}B^{**}_{(n-3)m(k-1)}(\rho,z)]\quad(n\geqslant 3). \tag{A21}$$

In [A18]–[A21],

$$R'_n(\rho,z-\mathrm{t})=\int B'_n(\rho,z-t)\,\mathrm{d}t=\frac{1}{n}B'_{n-1}(\rho,z-t), \tag{A22}$$

$$S'_n(\rho,z-t)=\int D'_n(\rho,z-t)\,\mathrm{d}t=\frac{1}{n}D'_{n-1}(\rho,z-t)+\frac{2}{n(n-1)}(z-t)B'_{n-2}(\rho,z-t), \tag{A23}$$

$$R''_n(\rho,z-t)=\int B''_n(\rho,z-t)\,\mathrm{d}t=\frac{1}{n}B''_{n-1}(\rho,z-t) \tag{A24}$$

and

$$S''_n(\rho,z-t)=\int D''_n(\rho,z-t)\,\mathrm{d}t=\frac{1}{n}D''_{n-1}(\rho,z-t)+\frac{2}{n(n-1)}(z-t)B''_{n-2}(\rho,z-t)$$
$$+\frac{2}{n(n-1)(n-2)}B''_{n-3}(\rho,z-t); \tag{A25}$$

and

$$B^{*}_{0m1}(\rho,z)=\frac{1}{\rho}[\rho^2+(z-t)^2]^{1/2}\Big|^{t_m}_{t_{m-1}}, \tag{A26}$$

$$B^{*}_{0m2}(\rho,z)=\left\{\frac{\rho}{2}\sinh^{-1}\frac{z-t}{\rho}-\frac{z-t}{2\rho}[\rho^2+(z-t)^2]^{1/2}\right\}^{t_m}_{t_{m-1}}+zB^{*}_{0m1}(\rho,z), \tag{A27}$$

$$B^{*}_{0m3}(\rho,z)=\left\{\frac{1}{3\rho}[\rho^2+(z-t)^2]^{3/2}-\rho[\rho^2+(z-t)^2]^{1/2}\right\}^{t_m}_{t_{m-1}}+2zB^{*}_{0m2}(\rho,z)-z^2B^{*}_{0m1}(\rho,z), \tag{A28}$$

$$D^{*}_{1m1}(\rho,z)=-\frac{z-t}{\rho}[\rho^2+(z-t)^2]^{1/2}\Big|^{t_m}_{t_{m-1}}, \tag{A29}$$

$$D^{*}_{1m2}(\rho,z)=\left\{\frac{2}{3\rho}[\rho^2+(z-t)^2]^{3/2}-\rho[\rho^2+(z-t)^2]^{1/2}\right\}^{t_m}_{t_{m-1}}+zD^{*}_{1m1}(\rho,z), \tag{A30}$$

$$B^{**}_{0m1}(\rho,z)=-\sinh^{-1}\frac{z-t}{\rho}\Big|^{t_m}_{t_{m-1}}, \tag{A31}$$

$$B^{**}_{0m2}(\rho,z)=[\rho^2+(z-t)^2]^{1/2}\Big|^{t_m}_{t_{m-1}}+zB^{**}_{0m1}(\rho,z), \tag{A32}$$

$$B^{**}_{0m3}(\rho,z)=\left\{\frac{\rho^2}{2}\sinh^{-1}\frac{z-t}{\rho}-\frac{z-t}{2}[\rho^2+(z-t)^2]^{1/2}\right\}^{t_m}_{t_{m-1}}+2zB^{**}_{0m2}(\rho,z)-z^2B^{**}_{0m1}(\rho,z), \tag{A33}$$

$$D^{**}_{2m1}(\rho,z)=\left\{\frac{z-t}{2}[\rho^2+(z-t)^2]^{-1/2}-\sinh^{-1}\frac{z-t}{\rho}\right\}^{t_m}_{t_{m-1}}, \tag{A34}$$

$$D^{**}_{2m2}(\rho,z)=\left\{[\rho^2+(z-t)^2]^{1/2}+\frac{\rho^2}{2}[\rho^2+(z-t)^2]^{-1/2}\right\}^{t_m}_{t_{m-1}}+zD^{**}_{2m1}(\rho,z) \tag{A35}$$

and

$$D^{**}_{2m3}(\rho, z) = \left\{\rho^2 \sinh^{-1}\frac{z-t}{\rho} - \frac{z-t}{2}[\rho^2+(z-t)^2]^{1/2} - \frac{\rho^2(z-t)}{2}[\rho^2+(z-t)^2]^{-1/2}\right\}_{t_{m-1}}^{t_m}$$
$$+ 2zD^{**}_{2m2}(\rho, z) - z^2 D^{**}_{2m1}(\rho, z). \quad [A36]$$

The following are the definitions of some functions used in section 8:

$$E'_{nmk}(\rho, z) = \int_0^{2\pi}\int_{\hat{\rho}_{m-1}}^{\hat{\rho}_m} \hat{\rho}^k \frac{\rho - \hat{\rho}\cos\hat{\phi}}{\rho^*}\beta'_n(\rho^*, z, 0)\,d\hat{\rho}\,d\hat{\phi} \quad [A37]$$

$$F'_{nmk}(\rho, z) = \int_0^{2\pi}\int_{\hat{\rho}_{m-1}}^{\hat{\rho}_m} \hat{\rho}^k \frac{\rho - \hat{\rho}\cos\hat{\phi}}{\rho^*}\delta'_n(\rho^*, z, 0)\,d\hat{\rho}\,d\hat{\phi} \quad [A38]$$

$$E''_{nmk}(\rho, z) = \int_0^{2\pi}\int_{\hat{\rho}_{m-1}}^{\hat{\rho}_m} \hat{\rho}^k \beta''_n(\rho^*, z, 0)\,d\hat{\rho}\,d\hat{\phi} \quad [A39]$$

$$F''_{nmk}(\rho, z) = \int_0^{2\pi}\int_{\hat{\rho}_{m-1}}^{\hat{\rho}_m} \hat{\rho}^k \delta''_n(\rho^*, z, 0)\,d\hat{\rho}\,d\hat{\phi} \quad [A40]$$

$$G'_{nmk}(\rho, z) = \int_0^{2\pi}\int_{\hat{\rho}_{m-1}}^{\hat{\rho}_m} \hat{\rho}^k \frac{\rho - \hat{\rho}\cos\hat{\phi}}{\rho^*}\alpha'_n(\rho^*, z, 0)\,d\hat{\rho}\,d\hat{\phi} \quad [A41]$$

$$H'_{nmk}(\rho, z) = \int_0^{2\pi}\int_{\hat{\rho}_{m-1}}^{\hat{\rho}_m} \hat{\rho}^k \frac{\rho - \hat{\rho}\cos\hat{\phi}}{\rho^*}\gamma'_n(\rho^*, z, 0)\,d\hat{\rho}\,d\hat{\phi} \quad [A42]$$

$$G''_{nmk}(\rho, z) = \int_0^{2\pi}\int_{\hat{\rho}_{m-1}}^{\hat{\rho}_m} \hat{\rho}^k \alpha''_n(\rho^*, z, 0)\,d\hat{\rho}\,d\hat{\phi} \quad [A43]$$

and

$$H''_{nmk}(\rho, z) = \int_0^{2\pi}\int_{\hat{\rho}_{m-1}}^{\hat{\rho}_m} \hat{\rho}^k \gamma''_n(\rho^*, z, 0)\,d\hat{\rho}\,d\hat{\phi} \quad [A44]$$

where $\rho^*$ is defined by [55], $n = 2, 3, \ldots, N+1$, $m = 1, 2, \ldots, M$ and $k = 1, 2, 3$. The integration in [A37]–[A44] can be performed numerically after the substitution of [21a–d] or [29a–d].